Mono-Higgs signature in the scotogenic model with Majorana dark matter

Amine Ahriche,[1,2,*] Abdesslam Arhrib,[3,†] Adil Jueid,[4,5,‡] Salah Nasri,[6,1,§] and Alejandro de la Puente[7,‖]

[1]*The Abdus Salam International Centre for Theoretical Physics, Strada Costiera 11, I-34014, Trieste, Italy*
[2]*Laboratoire de Physique des Particules et Physique Statistique, Ecole Normale Supérieure, BP 92 Vieux Kouba, DZ-16050 Algiers, Algeria*
[3]*Département des Mathématiques, Faculté des Sciences et Techniques, Université Abdelmalek Essaadi, Tanger B 416, Maroc*
[4]*INPAC, Shanghai Key Laboratory for Particle Physics and Cosmology, Department of Physics and Astronomy, Shanghai Jiao Tong University, Shanghai 200240, China*
[5]*Department of Physics, Konkuk University, Seoul 05029, Republic of Korea*
[6]*Department of Physics, United Arab Emirates University, Al-Ain 15551, United Arab Emirates*
[7]*New York Academy of Science, 7 World Trade Center, 250 Greenwich Street, 40th Floor, New York, New York 10007-2157, USA*

(Received 12 November 2019; accepted 5 February 2020; published 27 February 2020)

We study the phenomenology of the scotogenic model in the case of a Majorana dark matter (DM) candidate. This scenario gives important consequences since the parameter space of the model is almost unconstrained compared to the inert Higgs doublet model (or the scotogenic model with scalar DM) and hence offers new opportunities for discovery at future high energy colliders, e.g., the HL-LHC. As an example, we focus on the production of the Standard Model (SM) Higgs boson in association with a pair of dark scalars. Owing to its clean signature, the $\gamma\gamma$ decay channel of the SM Higgs boson is investigated in great detail at both the HL-LHC (at $\sqrt{s} = 14$ TeV) and the future FCC-hh (at $\sqrt{s} = 100$ TeV). After revisiting the LHC constraints from run II on the parameter space of the model and selecting benchmark points satisfying all the theoretical and experimental constraints, we found that scalars with mass up to 140 GeV (160 GeV) can be probed at the LHC (FCC-hh) with a 3 ab^{-1} of integrated luminosity assuming a total uncertainty of 5%.

DOI: 10.1103/PhysRevD.101.035038

I. INTRODUCTION

The observation of neutrino oscillations in solar, atmospheric, reactor, and accelerator experiments remains one clear indication that the Standard Model (SM) is not a complete framework of fundamental physics. The smallness of the observed neutrino masses tells us that at the nonrenormalizable level we might not have a straightforward answer to the mechanism that bestows neutrinos with mass. One popular mechanism for generating a tiny neutrino mass is the so-called seesaw mechanism [1–3]. However, realistic models based on the seesaw mechanism involve high mass scales that are hard to be probed at collider experiments. Neutrino mass generation through loop diagrams is interesting and gives *naturally* small masses due to loop-suppression factors. Therefore, these models can be probed at present and future colliders. In these classes of models, the smallness of the neutrino mass has been addressed within frameworks at one loop [4,5], two loops [6–10], three loops [11–26], and four loops [27].

Additionally, experimental evidence of dark matter (DM) has driven many years of investigation shedding light on possible particle and electroweak-size interaction explanations that can reproduce the observed DM relic abundance in the Universe. This paradigm is interesting since it can be tested at colliders such as the Large Hadron Collider (LHC). One of the simplest extensions of the SM consists in incorporating an additional inert Higgs doublet Φ with a discrete Z_2 symmetry under which the new scalar is odd, $\Phi \to -\Phi$, and the other SM fields are even [28]. In this case, the lightest odd particle would act as a DM candidate. This model, known as the inert Higgs doublet model (IHDM), contains one CP-even Higgs identified as the SM Higgs, another CP-even Higgs H^0, one CP-odd A^0, and a pair of charged Higgs $H^{\pm}$, and it consequently has a

*aahriche@ictp.it
†aarhrib@gmail.com
‡adiljueid@konkuk.ac.kr
§snasri@uaeu.ac.ae
‖lagrange2001@gmail.com

rich phenomenology [29–48]. For example, the model provides monojet, mono-Higgs, mono-Z, and monophoton signatures that can be tested at the LHC and future colliders. It appears from the above phenomenological studies that the IHDM is strongly constrained from direct and indirect DM searches, both for low and intermediate DM masses [39,49]. For DM lighter than 62.5 GeV, LHC data also put severe constraints on the invisible decay of the SM Higgs, which in turn translate into constraints on a combination of the scalar parameters of the potential [39,50]. Moreover, collider bounds on the IHDM are obtained as a reinterpretation of neutralino and chargino pair production both from LEP II [51] and from LHC [52]. From LEP II data, Ref. [51] sets an upper bound on the pseudoscalar mass, m_{A^0} (resp. m_{H^0}), below 100 GeV (resp. 80 GeV) consistent with mass splittings $\Delta m(A^0, H^0) \geq 8\,\text{GeV}$. While from LHC data, Ref. [52] limits have been derived using a dilepton plus missing energy signature which excludes masses for the exotic scalar up to 62.5 GeV. A recent study [50] showed that the LHC at 13 TeV and 3000 fb^{-1} luminosity could exclude exotic scalar masses below 83 GeV using the monojet channel.

However, if one focuses on a degenerate spectrum of exotic scalars, which is a natural outcome of accidental symmetries in the scalar potential [53], the region of scalar masses above $M_Z/2$ remains unconstrained for splittings between the exotic scalar and the charged scalar mass below 5 GeV. It was also found that LHC searches are not strong enough to probe the degenerate window due to lepton p_T requirements. In light of current collider experimental bounds and the viable region of parameter space in the IHDM, and in order to address the DM nature, one has to go beyond this minimal extension of the SM. For instance, extending the IHDM by three right-handed Majorana fermions may provide a possible solution to the problem of overconstrained quartic couplings and, on the other hand, give rise to small neutrino masses generated through one-loop diagrams. In the present work, we build on a recent phenomenological analysis in the framework of the scotogenic model [30] performed by some of us [54].[1] The scotogenic model is a SM minimal extension where the SM neutrinos obtain small masses at the one-loop order. In order to achieve this, the scalar potential has to be augmented by an inert complex scalar doublet with a small mixing quartic coupling to the SM Higgs. Due to the new Yukawa couplings, the scalar potential has an enhanced $SU(2)$ symmetry acting only on the exotic scalar and the new right-handed neutrino fields.[2] Because of this global symmetry, the quartic coupling λ_5 between Φ and the SM Higgs, which is responsible for the mass splitting between the CP-odd and CP-even neutral scalars, does not run and thus can naturally be very close to zero, which yields a small mass for the active neutrino. In contrast to the λ_5 term in the potential, there is another coupling between Φ and the SM Higgs, λ_4, which has a nonvanishing β function even if the coupling is chosen to be zero at some very high energy scale. This region of parameter space also corresponds to the spectrum of a compressed exotic scalar or pseudoscalar spectrum that leads to interesting collider signatures which are difficult to probe in the IHDM with current and near-future data.

In [54,60], the DM candidate is considered to be the lightest Majorana fermion N_1, which implies a significant difference in the parameter space compared to both IDHM and the scotogenic model with a scalar DM candidate. For instance, in the case of a scalar DM candidate, the null results from searches in direct detection imply that the coupling combination $\lambda_L = \lambda_3 + \lambda_4 + \lambda_5$ is extremely suppressed, while for the fermionic DM case this constraint does not affect the scalar potential's parameters. In the fermionic DM case, the CP-odd and CP-even scalars decay predominantly into the SM neutrino and the Majorana fermion N_i, and therefore they cannot be seen at colliders; i.e., they behave as dark scalars. In other words, both the IHDM and the scotogenic model provide identical signatures at colliders but with different event yields since they have different parameter space.

As pointed out above, the production of dark scalars can lead to several signatures dubbed as mono-X. The most well known and studied in the literature is the monojet signature. However, within the framework of the scotogenic model, the monojet signature is only sensitive to the masses of the particles produced in the final state and not to the scalar couplings such as, e.g., λ_L. The reason for this is that the monojet cross section gets its most important contribution from diagrams with the exchange of the Z boson and involving gauge couplings only. Therefore, alternatives to the monojet channel need to be exploited. In this regard, we focus on the mono-Higgs channel in the diphoton final state at both the HL option of the LHC at 14 TeV and the Future Circular Collider (FCC-hh) at 100 TeV. This signature is an excellent probe of new physics and DM [61–64]. We stress that searches of DM in events with Higgs and missing transverse energy have been carried out by the ATLAS and CMS collaborations [65–71] using $\tau^+\tau^-$, $\gamma\gamma$, and $b\bar{b}$ decay channels of the Higgs boson. These searches yielded null results which were used to put strong constraints on simplified models of DM production at hadron colliders. However, these limits do not apply to our model due to the smallness of the corresponding production cross sections of DM particles in association with a Higgs boson. In this work, we follow closely the analysis setup of Ref. [66]. The outline of the paper is as follow. In the second section we review the scotogenic model and all the theoretical and experimental bounds in

[1]The phenomenology of the scotogenic model has been extensively studied in the literature [55–59].

[2]This symmetry, however, is broken explicitly by the Majorana bare mass terms.

the entire degenerate window, where all exotic scalars have approximate equal masses. We then carry out a complete comparison of this model to the latest LHC run II data and expose the available parameter space in the third section. In the fourth and the fifth sections, we present a full sensitivity analysis to a mono-Higgs signature within this framework. The ATLAS and CMS searches of new physics we used in the reinterpretation part of the study are described in the Appendix.

II. THE MODEL: PARAMETERS AND CONSTRAINTS

A. Model

In this model, the SM is extended by one $SU(2)_L$ inert Higgs doublet and three singlet Majorana fermions $N_i \sim (1,1,0)$, $i = 1, 2, 3$. These new particles are odd under a Z_2 symmetry, whereas the SM particles are even. In this setup, the most general gauge-invariant and renormalizable scalar potential that is invariant under CP and Z_2 symmetries has the form

$$V = -\mu_1^2|H|^2 + \mu_2^2|\Phi|^2 + \frac{\lambda_1}{6}|H|^4 + \frac{\lambda_2}{6}|\Phi|^4 + \lambda_3|H|^2|\Phi|^2 + \frac{\lambda_4}{2}|H^\dagger\Phi|^2 + \frac{\lambda_5}{4}[(H^\dagger\Phi)^2 + \text{H.c.}]. \quad (1)$$

The electroweak symmetry breaking (EWSB) is achieved through the nonvanishing vacuum expectation value (VEV) acquired by the neutral component of the SM Higgs doublet, while the Z_2-odd inert doublet Φ does not develop a VEV as its quadratic term has positive curvature. The SM Higgs and the inert doublets can be parametrized as

$$H = \begin{pmatrix} G^+ \\ \frac{1}{\sqrt{2}}(v + h + iG^0) \end{pmatrix}, \qquad \Phi = \begin{pmatrix} H^+ \\ \frac{1}{\sqrt{2}}(H^0 + iA^0) \end{pmatrix}. \quad (2)$$

The Lagrangian that involves the Majorana fermions can be written as

$$\mathcal{L} \supset h_{\alpha j}\bar{L}_\alpha \epsilon \Phi N_j + \frac{1}{2}M_i \bar{N}_i^C N_i + \text{H.c.}, \quad (3)$$

where $\alpha = e, \mu, \tau$ stands for lepton flavors, $j = 1, 2, 3$ for singlet Majorana fermions, $\epsilon = i\sigma_2$ is an antisymmetric tensor, and $\bar{L}_\alpha$ is the left-handed lepton doublet. Note that the absence of $\bar{L}_{\alpha j} H N_j$ in the Lagrangian (3) is due to the imposed discrete Z_2 symmetry. The parameters λ_1 and μ_1^2 in (1) can be eliminated in favor of the SM Higgs mass and its VEV ($v = 246$ GeV). The expressions of λ_1 and μ_1^2 are considered at the one-loop level *à la* the $\overline{\text{DR}}$ scheme [72]. After EWSB, 3 degrees of freedom are absorbed by the longitudinal components of the gauge boson fields ($W^\pm$ and Z), and we are left with two CP-even scalars (h^0, H^0), one CP-odd scalar A^0, and a pair of charged scalars $H^\pm$. Their tree-level masses are given by

$$m_{H^\pm}^2 = \mu_2^2 + \frac{1}{2}\lambda_3 v^2, \quad m_{H^0,A^0}^2 = m_{H^\pm}^2 + \frac{1}{4}(\lambda_4 \pm \lambda_5)v^2. \quad (4)$$

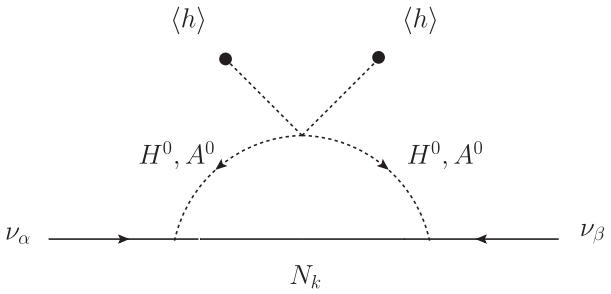

FIG. 1. Feynman diagram responsible for the neutrino mass.

The neutrino mass can be obtained at the one-loop level via the diagram in Fig. 1. The neutrino mass matrix elements [30,73] are given *à la* the Casas-Ibarra form [74] by

$$m_{\alpha\beta}^{(\nu)} = \sum_k h_{\alpha k} G_k h_{\beta k} = [h.G.h^T]_{\alpha\beta},$$
$$G_k = \frac{M_k}{16\pi^2}\left\{\frac{m_{H^0}^2}{m_{H^0}^2 - M_k^2}\ln\frac{m_{H^0}^2}{M_k^2} - \frac{m_{A^0}^2}{m_{A^0}^2 - M_k^2}\ln\frac{m_{A^0}^2}{M_k^2}\right\}. \quad (5)$$

In this model, the smallness of the neutrino mass is a consequence of the tiny mass splitting in the inert neutral sector. In other words, the ratio $\epsilon := \frac{|\lambda_5|v^2}{m_{H^0}^2 + m_{A^0}^2}$ is much smaller than unity. Then, after the expansion over ϵ, the parameter G_k in (5) is given by

$$G_k = \frac{|\lambda_5|}{16\pi^2}\frac{v^2}{\bar{m}}\left[\frac{x_k}{1 - x_k^2} + \frac{x_k^3}{(1 - x_k^2)^2}\ln x_k^2\right], \quad (6)$$

with $x_k = M_k/\bar{m}$ and $\bar{m}^2 = (m_{H^0}^2 + m_{A^0}^2)/2$. According to the Casas-Ibarra parametrization, the coupling h can be written as

$$h = D_{\sqrt{G_k}}\mathcal{R}D_{\sqrt{m_\nu}}U_\nu^T, \quad (7)$$

where $D_{\sqrt{G_k}} = \text{diag}\{\sqrt{G_1}, \sqrt{G_2}, \sqrt{G_3}\}$, $D_{\sqrt{m_\nu}} = \text{diag}\{\sqrt{m_1}, \sqrt{m_2}, \sqrt{m_3}\}$, $\mathcal{R}$ is an orthogonal rotation matrix ($m_{1,2,3}$ are the neutrino eigenmasses), and U_ν is the Pontecorvo-Maki-Nakawaga-Sakata (PMNS) mixing matrix [75] which is given by

$$U_\nu = \begin{pmatrix} c_{12}c_{13} & c_{13}s_{12} & s_{13}e^{-i\delta_d} \\ -c_{23}s_{12} - c_{12}s_{13}s_{23}e^{i\delta_d} & c_{12}c_{23} - s_{12}s_{13}s_{23}e^{i\delta_d} & c_{13}s_{23} \\ s_{12}s_{23} - c_{12}c_{23}s_{13}e^{i\delta_d} & -c_{12}s_{23} - c_{23}s_{12}s_{13}e^{i\delta_d} & c_{13}c_{23} \end{pmatrix} \times U_m, \tag{8}$$

where $s_{ij} \equiv \sin\theta_{ij}$, $c_{ij} \equiv \cos\theta_{ij}$ with θ_{ij} the mixing angles, δ_d represents the Dirac CP-violating phase, and $U_m = \mathrm{diag}(1, e^{i\theta_\alpha/2}, e^{i\theta_\beta/2})$. In this work we assume that U_ν is real-valued, which can be achieved by setting $\delta_d = \theta_\alpha = \theta_\beta = 0$. In our analysis, we constrain the parameters of the model by enforcing the computed neutrino mass matrix to satisfy the constraints from neutrino mixing angles and mass-squared differences, using the following values [76]:

$$s_{12}^2 = 0.320^{+0.016}_{-0.017}, \quad s_{23}^2 = 0.43 \pm 0.03,$$
$$s_{13}^2 = 0.025 \pm 0.003, \quad |\Delta m_{13}^2| = 2.55^{+0.06}_{-0.09} \times 10^{-3}\ \mathrm{eV}^2,$$
$$\Delta m_{21}^2 = 7.62^{+0.19}_{-0.19} \times 10^{-5}\ \mathrm{eV}^2.$$

In addition, we take into account the constraint from the nonobservation of neutrinoless double beta decay so that the contribution to such a process from the total lepton number violating interactions in the model is below the current experimental bound [77,78].

B. Constraints

The parameters of the scalar potential have to satisfy a number of theoretical and experimental constraints. On the theoretical side, we should require perturbativity of all the quartic couplings of the scalar fields. In addition, the scalar potential has to be bounded from below in all directions of the field space. For that, the necessary and sufficient conditions are given by [79]

$$\lambda_{1,2} > 0, \qquad \lambda_3 + \lambda_4 - |\lambda_5| + 2\sqrt{\lambda_1\lambda_2} > 0,$$
$$\lambda_3 + 2\sqrt{\lambda_1\lambda_2} > 0. \tag{9}$$

However, these constraints do not ensure the vacuum stability since the inert vacuum may not be the global minimum of the potential, and to guarantee this feature we should also impose the condition $\frac{\mu_1^2}{\sqrt{\lambda_1}} \geq -\frac{\mu_2^2}{\sqrt{\lambda_2}}$ [80]. Another set of constraints comes from the tree-level perturbative unitarity which should be preserved at high energies in a variety of processes involving scalars and/or gauge bosons. At high energies, using the equivalence theorem, we replace the longitudinal components of the W and Z bosons by the corresponding charged and neutral Goldstone bosons, respectively. Therefore, we are left only with pure scalar scattering amplitudes. Computing the decay amplitudes for these processes, one finds a set of four matrices with quartic couplings as their entries. The eigenvalues for those matrices have to be smaller than 4π [81,82].

Electroweak precision tests (EWPT) are a common approach to constrain physics beyond the SM by using the global fit through the oblique S, T, and U parameters [83]. In the scotogenic model, the new gauge-inert interactions induce nonvanishing contributions to the oblique parameters ΔT and ΔS [84].[3] To study the impact of the EWPT on the mass splitting between the pseudoscalar (A^0) and the charged Higgs boson ($H^\pm$), we use a χ^2-minimization procedure. The corresponding χ^2 is defined by

$$\chi^2 = \sum_{\mathcal{O}=S,T} \frac{(\mathcal{O} - \mathcal{O}_{\mathrm{exp}})^2}{\sigma_{\mathcal{O}}^2(1-\rho_{ST}^2)} - 2\rho_{ST}\frac{(S - S_{\mathrm{exp}})(T - T_{\mathrm{exp}})}{\sigma_S\sigma_T(1-\rho_{ST}^2)}, \tag{10}$$

with $S_{\mathrm{exp}} = 0.06 \pm 0.09$, $T_{\mathrm{exp}} = 0.10 \pm 0.07$ are the experimental values of the S and the T parameters, $\sigma_{S,T}$ are their corresponding errors, and $\rho_{ST} = +0.91$ is their correlation. The constraints from EWPT can be satisfied easily in regions of the parameter space where the mass splitting between the neutral and the charged components of the inert doublet is small (for light scalars) or where the scalars are very heavy regardless of the values of their mass splittings. In this model, constraints from neutrino masses and mixings imply extremely small values of λ_5. Therefore, the only parameter that is directly affected by the EWPT constraint is λ_4. In the left panel of Fig. 2, we display the 1-sigma ($\chi^2 < 2.3$), 2-sigma ($\chi^2 < 5.99$), and 3-sigma ($\chi^2 < 11.8$) allowed regions plotted in the $(m_{H^\pm}, \lambda_4)$ plane. We can see that, for e.g., $m_{H^\pm} \simeq 95$ GeV, λ_4 can vary in $[-0.2, 1.5]$, which implies a maximum mass splitting of about 100 GeV.

Moreover, the gauge boson decay widths are well measured [85] and must not be modified by any new interactions. Therefore, one needs to impose the conditions $m_{H^0} + m_{A^0}, 2m_{H^\pm} > M_Z$; $m_{H^\pm} + m_{A^0}, m_{H^\pm} + m_{H^0} > M_W$, to keep the decay channels of W and Z gauge bosons into inert particles closed.

The new Yukawa interactions in (3) lead to lepton flavor violating (LFV) decay processes that arise at the one-loop level with the exchange of charged Higgs $H^\pm$ and Majorana fermion N_k particles. The branching ratios of the decays $\ell_\alpha \to \ell_\beta + \gamma$ and $\ell_\alpha \to \ell_\beta\ell_\beta\ell_\beta$ are given in the literature

[3]The corrections to the U parameter in the IHDM are very small. Therefore, we assume that $\Delta U = 0$ in the present analysis.

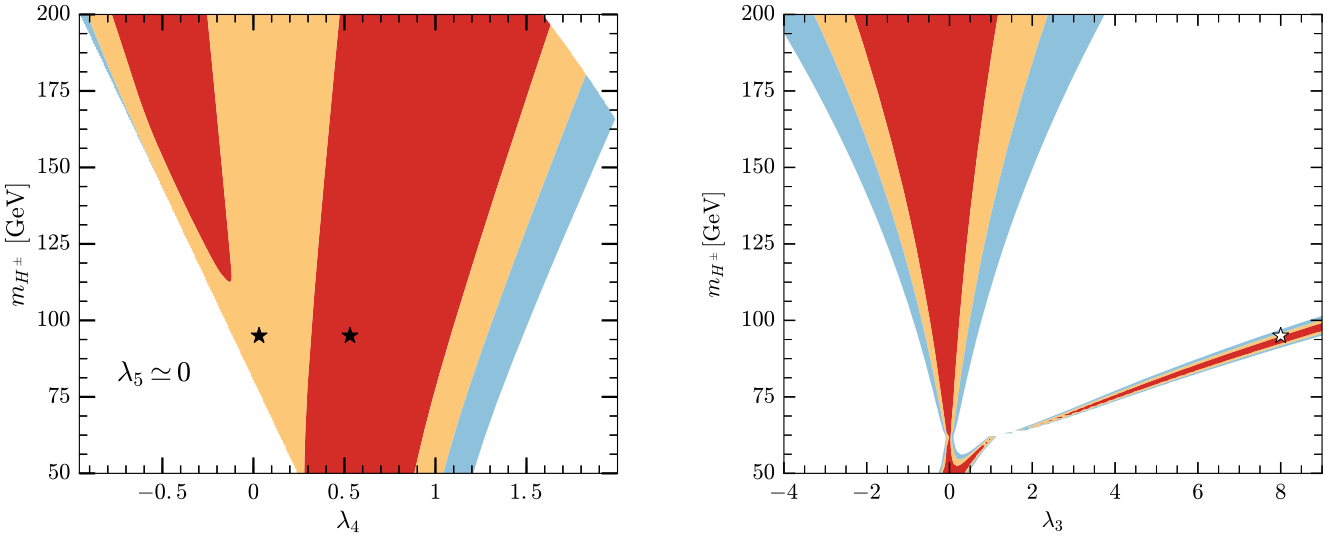

FIG. 2. Constraints on the model parameter space from oblique parameters in the mass of the charged Higgs mass and λ_4 (left) and from Higgs signal strength measurements in the charged Higgs mass and λ_4 (right). The red, yellow, and blue contours correspond to the 68%, 95%, and 99.7% allowed regions, respectively. Two different benchmark points corresponding to $(m_{H^\pm}, m_{A^0}) = (95, 100)$ GeV, $(95, 160)$ GeV are shown as black markers in the left panel. In the right panel, the white marker corresponds to the allowed value of λ_3, which we choose for the rest of the analysis. Due to the constraints from neutrino mass and mixing parameters, we have taken $\lambda_5 = 0$.

[86] and should be below the experimental bounds reported in [85]. The agreement of the chosen couplings $h_{\alpha k}$ with the LFV constraints can be moderated via a well-chosen matrix $\mathcal{R}$ in (7).

In the scotogenic model, all the SM Higgs couplings with SM particles are the same as in the SM except those relevant to the decays $H \to \gamma\gamma$ and $H \to \gamma Z$ which receive additional contributions from the charged Higgs bosons. Therefore, in the case where there is no large contribution to the invisible decay of the SM Higgs, most of the LHC measurements would fit pretty well within the scotogenic model. This is the case in our model; the only source of invisible decay is the one-loop induced coupling HN_iN_j which is suppressed in most regions of the parameter space. In the scotogenic model, the partial width of the SM Higgs boson in the $\gamma\gamma$ channel depends on the charged Higgs boson mass and λ_3. Positive (negative) values of the λ_3 would imply destructive (constructive) interferences with the leading W and the subleading top quark contributions [42]. Since the charged Higgs $H^\pm$ contribution would modify the rate through $H \to \gamma\gamma$, constraints from diphoton signal strength measurements at the LHC were taken into account as well. The public package LILITH [87,88] was used to check the constraints from various measurements of the Higgs boson signal strength ($\mu^i_{\gamma\gamma}$) defined by

$$\mu^i_{\gamma\gamma} = \frac{\sigma^i \Gamma(H \to \gamma\gamma)}{\sigma^i_{\rm SM} \Gamma(H \to \gamma\gamma)^{\rm SM}}, \tag{11}$$

where the superscript i refers to the production channel of the SM Higgs boson. In the right panel of Fig. 2, we plot the allowed regions from Higgs boson signal strength measurements in the $(\lambda_3, m_{H^\pm})$ plane. We can see that $\mu_{\gamma\gamma}$ strongly constrains the 2D parameter space. There are two notable regions for $m_{H^\pm} < 200$ GeV; the first one is centered around $\lambda_3 \simeq 0$ while the second one is a small segment corresponding to $\lambda_3 \in [0, 9]$ and $m_{H^\pm} < 100$ GeV. This is unsurprising because even for large positive values of λ_3, the $R_{\gamma\gamma}$ ratio in our model can still agree with data within the $+10\%$ of experimental uncertainty reported in e.g., the recent CMS analysis [89].

In this study, we assume that the lightest right-handed Majorana neutrino is a DM candidate as was done in Ref. [54]. For the light Majorana neutrinos (with masses up to 140 GeV) that we are interested in, the main annihilation channels are into charged leptons and SM neutrinos. These annihilation processes proceed through t-channel diagrams mediated by the members of the inert doublet. Furthermore, to simplify the collider analysis (see Secs. III and IV), nearly degenerate Majorana neutrinos are chosen, i.e., $m_{N_2} \simeq 1.01 m_{N_1}$ and $m_{N_3} \simeq 1.02 m_{N_1}$. In this case, coannihilation becomes important and, therefore, is included in our analysis. Coannihilation with inert scalars, which give rise to final states such as $\ell^\pm\gamma$, is subleading due to the smallness of the electromagnetic coupling compared to the new Yukawa couplings h_{ik} and can be safely neglected. Including all the significant channels, we select a benchmark point that is in agreement with the WMAP [90] and Planck [91] measurements of the relic density at the 2σ level.

In our model, DM can interact with the nucleons, and it triggers a possible signal in direct detection experiments.

The process of spin-independent (SI) DM-nucleus interactions occurs even though the $y_{hN_1N_1}$ coupling is not a tree-level one.[4] We estimate the SI scattering cross section of N_1 off a nucleon $\mathcal{N}$ and subject it to constraints from the void searches performed by Xenon1T [92]. One notices that constraints from direct detection are easily satisfied in our model due to the smallness of the $y_{hN_1N_1}$ coupling.

C. LEP constraints

Multiple searches for supersymmetric particles at e^+e^- collisions have been carried out by several collaborations [93–96] for center-of-mass energies of 183–209 GeV. These searches focused on chargino and neutralino pair production in events with two or three leptons and large transverse missing energy. Several interpretations in terms of models containing charged and neutral scalars have been made. Reference [51] made a comprehensive reinterpretation of neutralino pair production ($\chi_1^0\chi_2^0$) to constrain the production of H^0A^0 in the IHDM and obtained a limit $m_{A^0} > 100$ GeV for large mass splitting. Pair production of charginos ($\chi_1^+\chi_1^-$) was analyzed to put constraints on $H^\pm H^\mp$ production in a DM model with TeV scale colored particles [97] and in the compressed IHDM [53].

In this section, we study the impact of LEP searches on the parameter space of our model. For instance, LEP put strong bounds on the pair production cross section of neutralino pair production. However, these limits do not apply in the considered scenario of the scotogenic model because the tiny value of the coupling λ_5 (of order $10^{-8} - 10^{-10}$) required by the smallness of the neutrino masses forbids off-shell decays, such as $A^0 \to H^0 Z \to H^0 \ell\ell$, and therefore yields an undetected final state. However, limits from chargino pair production can be applied to our model. Two processes can be used for such constraints: $e^+e^- \to H^+H^-$ and $e^+e^- \to H^0A^0$. The latter contribute, if $\lambda_4 > 0$ and $\Delta_{H^\pm H^0} = m_{A^0,H^0} - m_{H^\pm} > m_{e,\mu}$, through off-shell decays. This contribution is proportional to $(\Delta_{H^\pm H^0})^5$ and, hence, is very small. Therefore, charged Higgs pair production is the only process for which the exclusion limits from LEP searches can be used to constrain our model. We consider the results of the searches carried out by OPAL [95] at $\sqrt{s} = 208$ GeV and $\mathcal{L} = 680$ pb^{-1} of integrated luminosity to derive conservative limits on the model parameter space, i.e., by assuming that the efficiency of the selection is 100%.[5]

The pair production of the charged particle depends on new Yukawa couplings and the gauge couplings. The first contribution is proportional to

$$\sum_{k=1}^{3} |h_{ek}|^2 = |h_{e1}|^2 + |h_{e2}|^2 + |h_{e3}|^2, \tag{12}$$

in the case of degenerate Majorana fermions. Because for $\lambda_4 \geq 0$ the charged Higgs boson decays with a 100% branching ratio into $N_k\ell$, the limits from chargino searches can be used to constrain both the charged Higgs boson and the mass splitting $\Delta_{H^\pm}$ defined by

$$\Delta_{H^\pm} = m_{H^\pm} - m_{N_1}. \tag{13}$$

We consider two scenarios for the new Yukawa couplings: (1) where the Yukawa matrix is chosen as follows,

$$h_{\alpha j} = 10^{-2} \begin{pmatrix} -60.86 - i0.20 & -0.30 - i0.80 & 14.49 - i0.75 \\ 25.14 - i0.57 & -1.12 - i2.49 & 40.87 + i0.24 \\ 3.70 + i0.62 & 1.10 + i3.88 & -44.20 + i0.14 \end{pmatrix}, \tag{14}$$

which we call the first scenario, and (2) where the coupling combination in Eq. (12) is larger than the case of the first scenario, while h_{ek} are still in agreement with all the theoretical and experimental constraints ($h_{e1} = -0.026 + i0.042$, $h_{e2} = 2.22 - i0.081$, $h_{e3} = 0.32 - i0.0098$). Notice that the charged Higgs bosons decay with a branching ratio of 100% into $N_k\ell$, and the new Yukawa matrix elements h_{ek}, $k = 1, 2, 3$ are the only parameters sensitive to LEP constraints.

In order to study the impact of the null results of the LEP searches on the parameter space of our model, we compute the $r_{95\%}(X_0)$ ratio defined by

$$\begin{aligned} r_{95\%} &\equiv r_{95\%}(X_0, h_{\alpha j}) \\ &= \frac{\sigma_{e^+e^-\to H^+H^-}(X_0, h_{ej}) \times \mathrm{BR}^2_{H^\pm \to N_k \ell^\pm}(X_0, h_{\alpha j})}{\sigma^{\mathrm{obs.}}_{95\%}(X_0)}, \\ &= \frac{\sigma_{e^+e^-\to H^+H^-}(X_0, h_{ej})}{\sigma^{\mathrm{obs.}}_{95\%}(X_0)}, \end{aligned} \tag{15}$$

where $\sigma^{\mathrm{obs.}}_{95\%}(X_0)$ is the 95% CL observed upper bound on the production cross section for the benchmark point $X_0 = (m_{H^\pm}, \Delta_{H^\pm})$. In the second line of Eq. (15), we have used $\mathrm{BR}(H^\pm \to \ell^\pm N_k) = 1$ since the semivisible decay

[4]However, radiative corrections generate such couplings at the one-loop order (see, e.g., [54] for more details).

[5]A full analysis of the signal process at the detector level will yield an efficiency that is always smaller than 100%. Therefore, the limits we obtain in this study are more conservative.

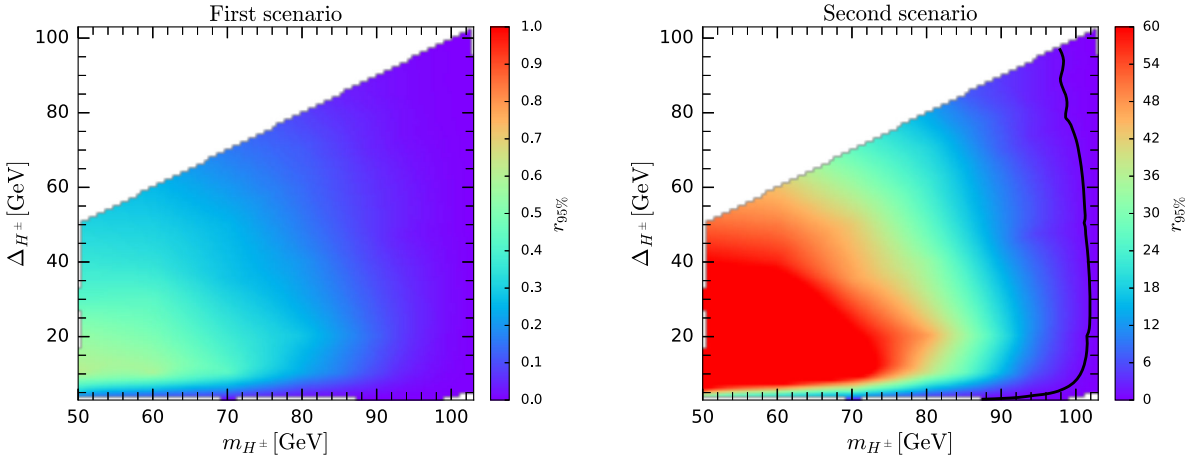

FIG. 3. Results of reinterpretation of LEP searches of chargino pair production on the $(\Delta_{H^\pm}, m_{H^\pm})$ plan in the first scenario (left) and second scenario (right).

$H^0/A^0 \to H^\pm W^\pm$ is closed due to the choice $m_{H^0} - m_{H^\pm} > M_W$. Note that the observed limit on the cross section does not depend on $h_{\alpha j}$, while the predicted cross section does. The null results of the searches for chargino pair production imply that a particular benchmark point (X_0, h_{ej}) is excluded if the production cross section in our model is larger than the upper limit reported by LEP-II and, therefore, if $r_{95\%} > 1$. In Fig. 3, we depict the exclusions from chargino pair production in the $(m_{H^\pm}, \Delta_{H^\pm})$ plane. As can be seen from the left panel of Fig. 3, all points are allowed by LEP searches. However, in the second scenario, one notices that the model is excluded for $m_{H^\pm} < 100$ GeV. A small window corresponding to $\Delta_{H^\pm} < 5$ GeV and 90 GeV $< m_{H^\pm} < 100$ GeV is still allowed by these constraints.

III. CONSTRAINTS FROM LHC SEARCHES AT 13 TEV

The model parameter space can be constrained by reinterpreting several ATLAS and CMS searches for new physics beyond the SM. In this study, we use the public tool CheckMate [98–102], which is dedicated to the reinterpretation of LHC searches of new physics. Degenerate Majorana neutrinos are chosen to avoid the possibility for displaced vertices. The other parameters are fixed to avoid all the other theoretical and experimental constraints [54], and they are chosen to be

$$\lambda_3 = 8, \qquad m_{H^\pm} = 95 \text{ GeV},$$
$$m_{H^0} \in [100, 200] \text{ GeV}, \quad \text{and} \quad m_{N_k} < m_{H^0}. \quad (16)$$

The LHC searches used in this analysis are displayed in Table I. The model parameter space can be affected by the LHC searches displayed in Table I as we will show explicitly. Details about the different searches performed at the LHC and the model-dependent processes that are sensitive to them are reported in the Appendix.

In our model, new sources of missing transverse energy E_T^{miss}, namely, from right-handed neutrinos N_i, exist. These new sources can be probed at colliders with events triggered by large missing E_T^{miss}. However, Majorana neutrinos cannot be produced directly because of the absence of the vertices $Z^0 N\bar{N}$, $\gamma N\bar{N}$, and $HN\bar{N}$; right-handed neutrinos are thus produced via the decays of the exotic scalars.

In the degenerate window, since the decay $A^0 \to H^0 Z^0$ is kinematically forbidden, the scalar or pseudoscalar can be produced in association with a charged scalar, which subsequently decays to a charged lepton and a right-handed neutrino. While the scalar and pseudoscalar may only decay invisibly, we obtain a signal with a single lepton and large missing E_T^{miss}. In this channel the most sensitive LHC search comes from the work in [103], which searches for SUSY in a final state with one isolated lepton. In the case where the exotic scalars are pair produced, in the

TABLE I. A selected set of ATLAS and CMS searches that were used in the reinterpretation study. These analyses are implemented in CheckMate.

Analysis	Experiment	Luminosity (fb^{-1})	Reference
atlas_conf_2016_050	ATLAS	13.3	[103]
atlas_conf_2016_066	ATLAS	13.3	[104]
atlas_conf_2016_076	ATLAS	13.3	[105]
atlas_conf_2017_060	ATLAS	36.1	[106]
atlas_1704_03848	ATLAS	36.1	[107]
atlas_1709_04183	ATLAS	36.1	[108]
atlas_1712_02332	ATLAS	36.1	[109]
atlas_1712_08119	ATLAS	36.1	[110]
atlas_1802_03158	ATLAS	36.1	[111]
cms_sus_16_025	CMS	12.9	[112]
cms_sus_16_039	CMS	35.6	[113]
cms_sus_16_048	CMS	35.9	[114]

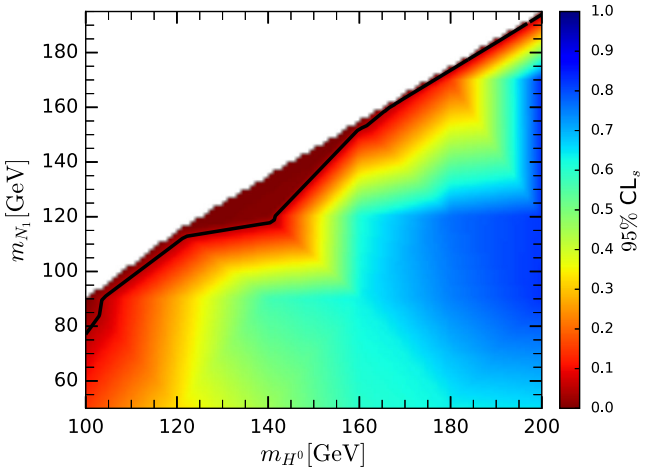

FIG. 4. Exclusions from LHC searches for new physics at $\sqrt{s} = 13$ TeV projected on the (m_{H^0}, m_{N_1}) plane. The color map shows the CL$_s$ values. The area above the black line shows the excluded regions corresponding to CL$_s < 0.05$. The white shaded area corresponds to both the regions that are forbidden by the kinematical constraint $m_{H^0} > m_{N_1}$ and the regions with CL$_s <$ 0.05 (since any region above the black line is already excluded).

degenerate region, their decays lead only to missing E_T^{miss}, and one can tag this channel with a monojet from initial state radiation. In these cases, LHC searches with photons and jets are the most sensitive, with the largest amount of missing E_T^{miss} found when the scalar or pseudoscalar mass approaches the right-handed neutrino mass, and this is where the bulk of the exclusion lies as can be seen from Fig. 4 after the inclusion of all relevant LHC searches given in Table I. Following the results of the reinterpretation of LHC searches of new physics that we have shown in Fig. 4, we choose the following benchmark points for the mono-Higgs study:

$$100\ \text{GeV} \leq m_{H^0} = m_{A^0} \leq 200\ \text{GeV}, \qquad m_{H^\pm} = 95\ \text{GeV},$$
$$m_{N_1} = m_{N_2} = m_{N_3} = 80\ \text{GeV}, \qquad \lambda_3 = 8, \tag{17}$$

while the new Yukawa couplings are fixed to their values shown in Eq. (14).

IV. MONO-HIGGS SIGNATURE

In this section, we describe different aspects of our analysis. First we discuss the different parton level contributions to the signal process as well as the possible backgrounds and the corresponding cross sections in the case of the $\gamma\gamma + E_T^{\text{miss}}$ reconstructed final state. Then, we discuss in depth the phenomenological setup used in our analysis and event selection.

A. Signal and backgrounds

In this model, mono-Higgs production proceeds through two different processes, i.e.,

$$pp \to SSH \to N_i N_j \nu\bar{\nu} H \tag{18}$$

and

$$pp \to N_i N_j H. \tag{19}$$

The corresponding Feynman diagrams are depicted in Fig. 5. There are four contributions to the Higgs $+ E_T^{\text{miss}}$ signal in hadronic collisions which involve either the production of an off-shell Higgs boson or a Z boson. In Fig. 5(a), the off-shell Higgs boson splits into SSH, while in Fig. 5(b), it involves a contribution from the SM Higgs trilinear coupling λ_{HHH}. In Fig. 5(c), $q\bar{q}$ annihilates into a Z^* which splits into two dark Higgses. In Fig. 5(d), the contribution consists of two Majorana neutrinos produced

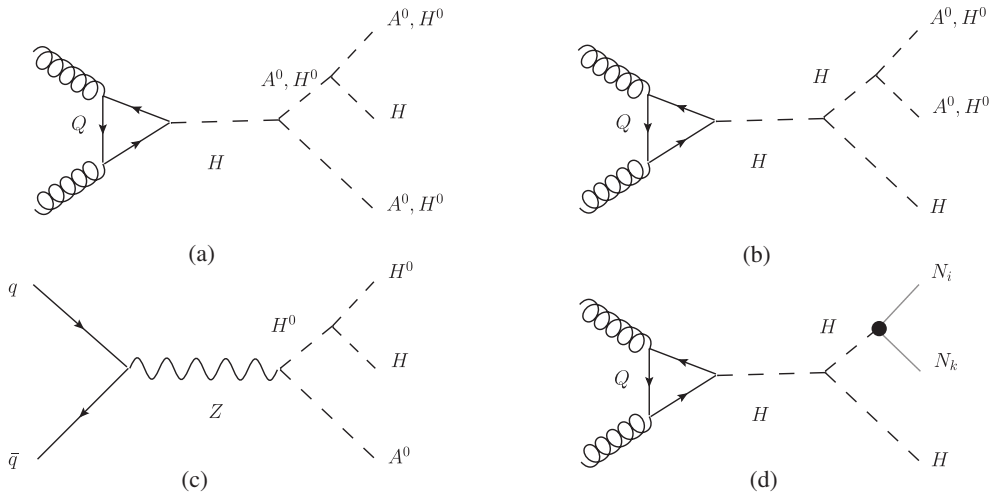

FIG. 5. Parton level Feynman diagrams contributing to the mono-Higgs signal in hadronic collisions. Unlike the fourth diagram, the first three diagrams are efficient only when the decays $H^0/A^0 \to W^\pm H^\mp$ have extremely small branching fractions.

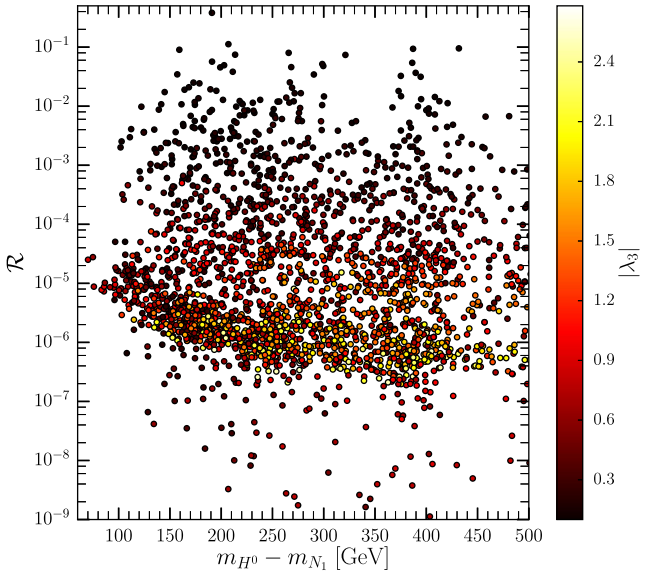

FIG. 6. $\mathcal{R}$, defined in Eq. (21), as a function of $m_{H^0} - m_{N_1}$. The color map shows the values of $|\lambda_L|$. The points shown in the plot satisfy all the theoretical and experimental constraints discussed in Sec. II.

in association with a SM Higgs boson. The first and second contributions interfere destructively (constructively) for negative (positive) values of the HSS couplings. We notice that the contribution of Fig. 5(c) contributes about 95% of the total cross section. This is unsurprising since this contribution occurs at the tree level and is enhanced for large values of λ_L. Using simple power counting, one notices that the total cross section behaves as

$$\sigma \propto |\lambda_L^2 \mathcal{M}_a + \lambda_L \lambda_{HHH} \mathcal{M}_b|^2 + |\lambda_L \mathcal{M}_c|^2 + |\sum_{i,j=1}^{3} \tilde{y}_{HN_iN_j} \lambda_{HHH} \mathcal{M}_d|^2. \quad (20)$$

The contribution of Fig. 5(d) is proportional to the square of the HN_iN_j coupling, which is one-loop induced [54], and it is expected to be very small. In this regard, we define the ratio $\mathcal{R}$ by

$$\mathcal{R} = \frac{\sum_{i,j=1}^{3} |\tilde{y}_{HN_iN_j}|^2}{|\lambda_L|^4}, \quad (21)$$

which gives a rough estimate of the relative contribution of Fig. 5(d) to the signal cross section, where only the leading contribution to SSH production ($\simeq|\lambda_L|^4$) is included. We show this ratio in Fig. 6 as a function of the mass splitting $\Delta m_{NH^0} = m_{H^0} - m_{N_k}$ with a color map showing $|\lambda_3|$. One can see that this ratio can only be important for very small values of λ_L, i.e., $|\lambda_L| < 0.1$. Given that this region is not interesting from a phenomenological point of view as it yields very small cross sections, we conclude that the contribution of Fig. 5(d) can be safely neglected.

The cross section for the mono-Higgs production is depicted in the left panel of Fig. 7. As expected, one can see that the cross section is pretty small for the LHC at $\sqrt{s} = 14$ TeV with the maximum being $\sigma_{\max} \simeq 53$ fb for $m_{H^0} = 100$ GeV, which increases by about an order of magnitude at the FCC-hh with 100 TeV. Since the mass splitting $\Delta_{H^\pm H^0}$ can be as large as 100 GeV, the dark neutral (pseudo)scalar does not always decay exclusively into an invisible final state. Therefore, in order to correctly estimate the number of events in a signal benchmark point, one has

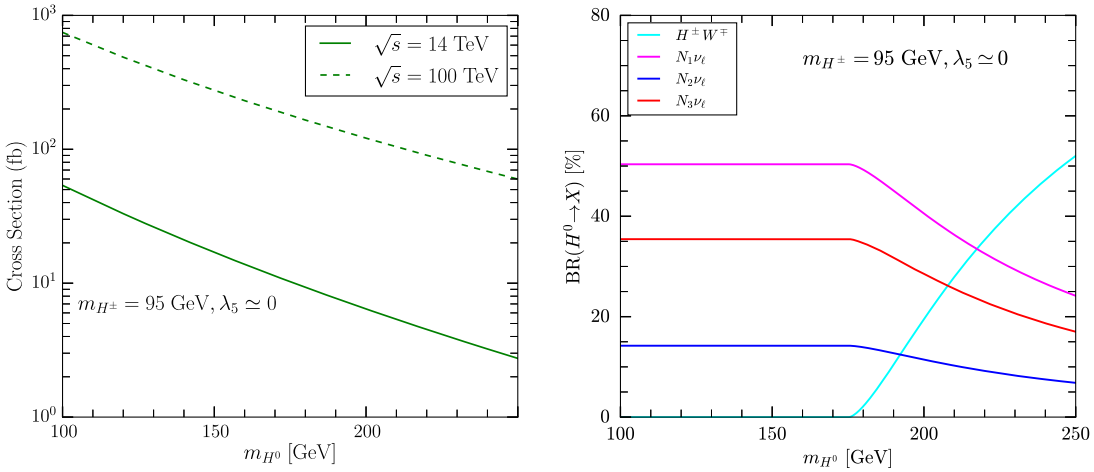

FIG. 7. Left: Mono-Higgs boson production cross section as a function of the dark scalar mass $m_{H^0} \simeq m_{A^0}$ for $m_{H^\pm} = 95$ GeV at the LHC (solid line) and at a future 100 TeV collider (dashed line). We include the processes $gg \to H^0H^0H$, $gg \to A^0A^0H$, and $q\bar{q} \to H^0A^0H$. The depicted results were LO computed with MadGraph5_aMC@NLO. Right: Decay branching ratios of the dark scalar particle as a function of the dark scalar mass for the values of the new Yukawa couplings shown in Eq. (14) and for $m_{N_1} = m_{N_2} = m_{N_2} = 80$ GeV.

TABLE II. Cross sections for processes contributing to the Higgs + E_T^{miss} background. The numbers outside (inside) the brackets refer to the rates at 14 (100) TeV. Details about the computation are explained in the text. Here, $\sigma \times \text{BR}$ refers to $\sigma(gg \to H) \times \text{BR}(H \to \gamma\gamma)$ for $gg \to H$, to $\sigma(pp \to ZH) \times \text{BR}(H \to \gamma\gamma) \times \text{BR}(Z \to \bar{\nu_\ell}\nu_\ell)$ for ZH, to $\sigma(pp \to W^{\pm}H) \times \text{BR}(H \to \gamma\gamma) \times \text{BR}(W^{\pm} \to \ell^{\pm}\nu_\ell)$ for the case of $W^{\pm}H$, and to $\sigma(pp \to W^{\pm} + n\gamma) \times \text{BR}(W^{\pm} \to \ell^{\pm}\nu_\ell) + \sigma(pp \to Z + n\gamma) \times \text{BR}(Z \to \bar{\nu}_\ell\nu_\ell)$ for $V + n\gamma, n = 1, 2$.

Process	$\sigma \times$ BR [fb]	Generator	Perturbative order
$gg \to H$	$128.54(1.94 \times 10^3)$	SusHi [115,116]	NNNLO
$W^{\pm}H$	1.16(12.59)	VH@NNLO [125]	NNLO
ZH	0.52(7.34)	VH@NNLO [125]	NNLO
$V\gamma\gamma$	51.99(621.96)	MadGraph5_aMC@NLO [127]	NLO
$V\gamma$	$42.89 \times 10^3(397.04 \times 10^3)$	MadGraph5_aMC@NLO [127]	NLO
$\gamma\gamma$ + jets	$4.19 \times 10^6(52.81 \times 10^6)$	SHERPA [129]	NLO

to correctly scale the corresponding cross section by $\text{BR}(H^0 \to \text{invisible})^2$. We show the dark scalar branching ratios as a function of m_{H^0} in Fig. 7 (right). We can see that, unless $m_{H^0} > 190$ GeV, the invisible decays of H^0 always have a branching fraction larger than 90%.

The $\gamma\gamma$ decay channel represents a very clean signature of the mono-Higgs final-state boson despite the smallness of the corresponding branching ratio (which is about $\simeq$0.23%). In this case, the following backgrounds have to be considered.

(i) $gg \to H \to \gamma\gamma$: In this background, the presence of missing energy is due to the misidentification of soft QCD radiation. However, it can be substantially suppressed by requiring high missing transverse energy as we will show later.

(ii) $pp \to ZH$: Here, the Z boson decays to a pair of neutrinos, which is an irreducible background. The suppression of this background can be achieved by applying specific selection criteria, e.g., on the transverse mass of the (Higgs, E_T^{miss}) system.

(iii) $pp \to W^{\pm}H$: Here, the $W^{\pm}$ boson decays into $\ell^{\pm}\nu$, where the charged lepton escapes detection, i.e., not passing the selection threshold. At the LHC, the charged lepton efficiency is high, and therefore, we expect that this background will have a small contribution.

(iv) $pp \to V\gamma\gamma$: Here, the $V = Z$ boson decays invisibly, and the $V = W$ boson decays leptonically. The $Z\gamma\gamma$ background is irreducible, contrarily to the $W\gamma\gamma$. The contribution of the latter can be reduced by imposing a lepton veto in the selection procedure. Both backgrounds have a weaker p_T spectrum of the identified photons. Therefore, their contribution can be reduced by strong requirements on the p_T^{γ} and the invariant mass of the $\gamma\gamma$ spectrum.

(v) $pp \to V\gamma$: This background is similar to $V\gamma\gamma$.

(vi) $pp \to \gamma\gamma$ + jets: In the hadronic environment, there is a possibility that pileup events will contribute to fake high missing transverse energy. The rate of this process is very high, and we opt to generate parton level cross sections with some cuts on the p_T of photons and jets. The ATLAS [66] and CMS [71] collaborations used different strategies to reduce the contribution of this background, either by defining some kinematical variables or by using azimuthal separation between the reconstructed Higgs candidate and the missing transverse energy. These features will be discussed briefly in the next subsection.

B. Phenomenological setup and event selection

The cross sections of the background processes are depicted in Table II for both the LHC at $\sqrt{s} = 14$ TeV and FCC-hh at $\sqrt{s} = 100$ TeV. The cross section of $gg \to H$ was computed at NNNLO using SusHi [115,116] version 1.6.1, which implements the results of [117–121]. The rates for the $W^{\pm}H$ and ZH processes were estimated at NNLO [118,122], including NLO EW corrections [123] and top quark mass effects [124], using the public package VH@NNLO [125] version 2.0.3. In all the NNLO calculations, the CT10 PDF set [126] was used with $\alpha_s(M_Z^2) = 0.118$. The cross section for $V\gamma$ and $V\gamma\gamma$ was evaluated at NLO using MadGraph5_aMC@NLO [127] with the NNPDF30 PDF sets [128]. The estimate of the $\gamma\gamma$ process (excluding the H contribution) was done using SHERPA version 2.2.5 [129], where inclusive samples of multiplicity up to four jets in the final state are merged using the CKKW matching scheme [130] and a merging scale $Q_0 = 20$ GeV.

Events for both the signal and the backgrounds were generated using MadGraph5_aMC@NLO and PYTHIA8 [131] at LO in QCD. Background events involving the Higgs boson were generated and decayed with PYTHIA8, while $V\gamma$ and $V\gamma\gamma$ events were generated using MadGraph5_aMC@NLO including the leptonic decays of the massive electroweak gauge bosons. The $\gamma\gamma$ + jets events were generated with PYTHIA and normalized to their rate at NLO. Since the rate of this process is huge, and most of the events will be vetoed in the initial selection, events are generated with a $p_{T,\gamma}^{\text{min}} = 70$ GeV, and $|\eta^{\gamma}| < 2.5$. Events for $gg \to H$ were scaled by a K factor of 3.2 using the results of SusHi, while VH events were scaled by a factor of 1.6. All the

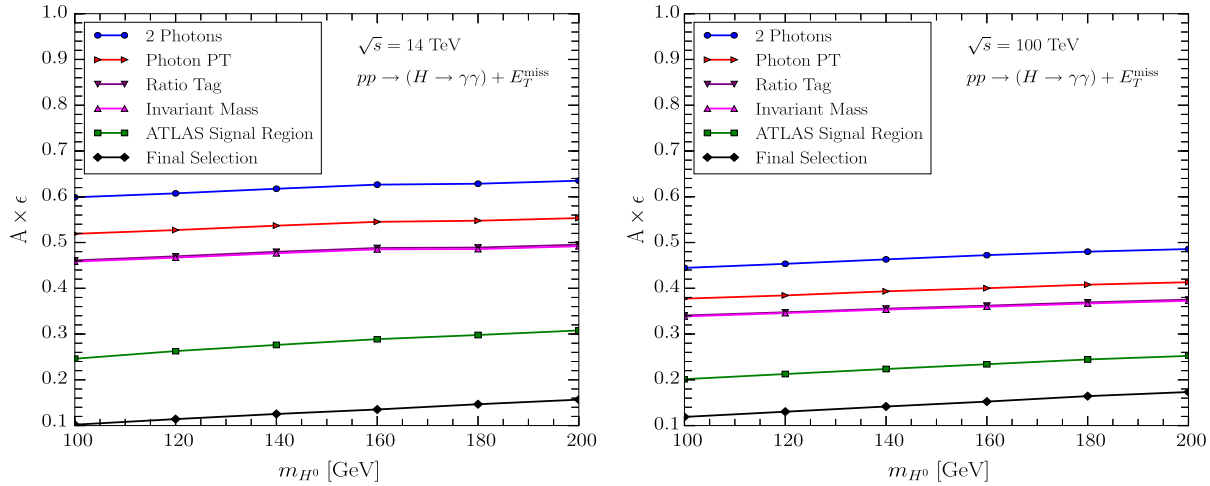

FIG. 8. The acceptance times the efficiency ($A \times \epsilon$) for the signal after each step of the event selection as a function of the dark Higgs mass for $\sqrt{s} = 14$ TeV (left) and $\sqrt{s} = 100$ TeV (right). We show $A \times \epsilon$ after the "2 Photons" selection step (blue), for the events passing the "Photon PT" selection (red), after the photon isolation selection denoted by "Ratio Tag" (purple) and for events in which the invariant mass of the diphoton system falls in the interval $m_{\gamma\gamma} \in [110, 160]$ GeV (rose). The efficiencies for the two signal regions are shown in green (ATLAS signal region) and in black (tight selection).

TABLE III. Cut flow for the $H \to \gamma\gamma$ final state at the LHC at $\sqrt{s} = 14$ TeV and for 3 ab^{-1} of luminosity.

Cuts	SM Higgs	$V\gamma\gamma$, $V\gamma$	$\gamma\gamma$ + jets	Signal	S/B
Initial events	322359	128432167	24030000	365	2.4×10^{-6}
2 photons	168005	2548352	6837913	218	2.3×10^{-5}
Photon PT	150570	1177335	6317283	189	2.5×10^{-5}
Ratio tag	135720	830147	5582001	168	2.6×10^{-5}
Invariant mass	135492	174358	2066511	166	6.9×10^{-5}
ATLAS signal region	98	151	0	89	0.35
Final selection	29	5	0	32	0.94

TABLE IV. Cut flow for the $H \to \gamma\gamma$ final state at the LHC at $\sqrt{s} = 100$ TeV and for 3 ab^{-1} of luminosity.

Cuts	SM Higgs	$V\gamma\gamma$, $V\gamma$	$\gamma\gamma$ + jets	Signal	S/B
Initial events	5885817	1192995664	252090000	5147	3.5×10^{-6}
2 photons	2597337	18298491	73202377	2287	2.4×10^{-5}
Photon PT	2272845	8405387	67325991	1941	2.5×10^{-5}
Ratio tag	2051298	6134810	59189681	1753	2.6×10^{-5}
Invariant mass	2048497	1228567	21714801	1741	6.9×10^{-5}
ATLAS signal region	4882	1889	0	1036	0.15
Final selection	2215	315	0	612	0.24

TABLE V. Selection rule used to enhance the significance for the $H(\to\gamma\gamma) + E_T^{\rm miss}$ final state.

Signal region	Cuts
ATLAS signal region	$p_T^{\gamma\gamma} > 90$ GeV, $S_{E_T^{\rm miss}} > 7$.
Tight selection	$p_T^{\gamma\gamma} > 90$ GeV, $S_{E_T^{\rm miss}} > 7$, $E_T^{\rm miss} > 200$ GeV, p_T^{γ}(lead) > 40 GeV

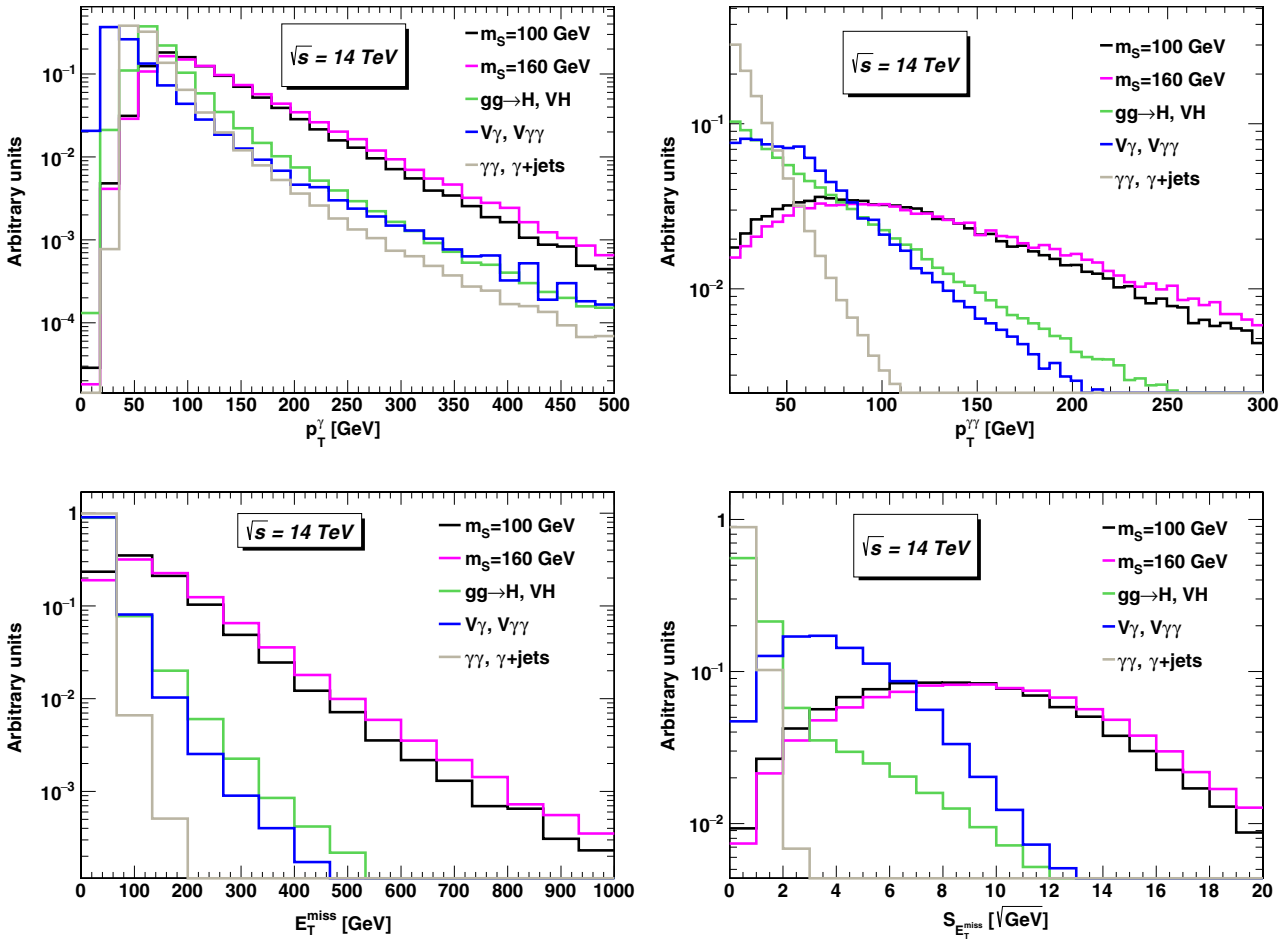

FIG. 9. Normalized distributions for the signal and the backgrounds at $\sqrt{s} = 14$ TeV. Here, we show the transverse momentum of the leading photon p_T^γ (top left), the transverse momentum of the diphoton system $p_T^{\gamma\gamma}$ (top right), missing transverse energy E_T^{miss} (bottom left), and the $S_{E_T^{\text{miss}}}$ defined in Eq. (22) (bottom right). The color coding is a follows: SM Higgs processes are shown in green, $V\gamma$ and $V\gamma\gamma$ are shown in blue, and $\gamma\gamma + \text{jets}$ are shown in gray. We show here the signal for $m_{H^0} = 100$ GeV (black) and $m_{H^0} = 160$ GeV (rose).

background events were showered with PYTHIA. DELPHES3 was used for fast detector simulation [132].

The analysis of events was carried out at the detector level using implemented efficiencies, and misidentification rates in DELPHES where the parameters are tuned for the ATLAS experiment and extrapolated for a future FCC-hh [133]. Events pass a preselection stage where all the objects (leptons, jets, photons, and missing E_T) are kept. The acceptance times the efficiency ($A \times \epsilon$) is depicted in Fig. 8 as a function of m_{H^0} for $\sqrt{s} = 14$ TeV and $\sqrt{s} = 100$ TeV. The cut flow for the event selection is shown in Tables III and IV. Events are selected if they contain at least two photons with $p_T^\gamma > 25$ GeV and $|\eta^\gamma| < 2.37$. This selection is denoted by "Photon PT" in Fig. 8 and Tables III and IV. In addition, we do not impose any requirement on the multiplicity, hardness, and flavor compositions of jets or the multiplicity of charged leptons. The photons that pass the initial selection will be subject to further isolation cuts (as in [66]), and the photon candidates are ordered by their transverse momentum. The two leading photons are used to reconstruct a Higgs candidate. Further, the ratio of the transverse momentum to the invariant mass $p_T^\gamma/m_{\gamma\gamma}$ is required to be larger than 0.35 (0.25) for the leading (subleading) photon. Moreover, a cut on the invariant mass of the diphoton system is imposed; namely, events are selected if $110\ \text{GeV} < m_{\gamma\gamma} < 160\ \text{GeV}$. In some cases, events in the $\gamma\gamma$ and $\gamma + \text{jets}$ backgrounds contain large fake transverse missing energy, which is due to the fact that, in such events, the vertex with larger $\sum p_T^2$ (where the sum runs over all the tracks) does not come from the primary vertex but from the pileup.[6] Both the ATLAS and CMS collaborations used sophisticated methods to reduce the contribution of pileup to missing transverse energy. The ATLAS Collaboration has defined a new variable $S_{E_T^{\text{miss}}}$ as

[6]A primary vertex is defined as the spatial point where proton-proton collisions occur.

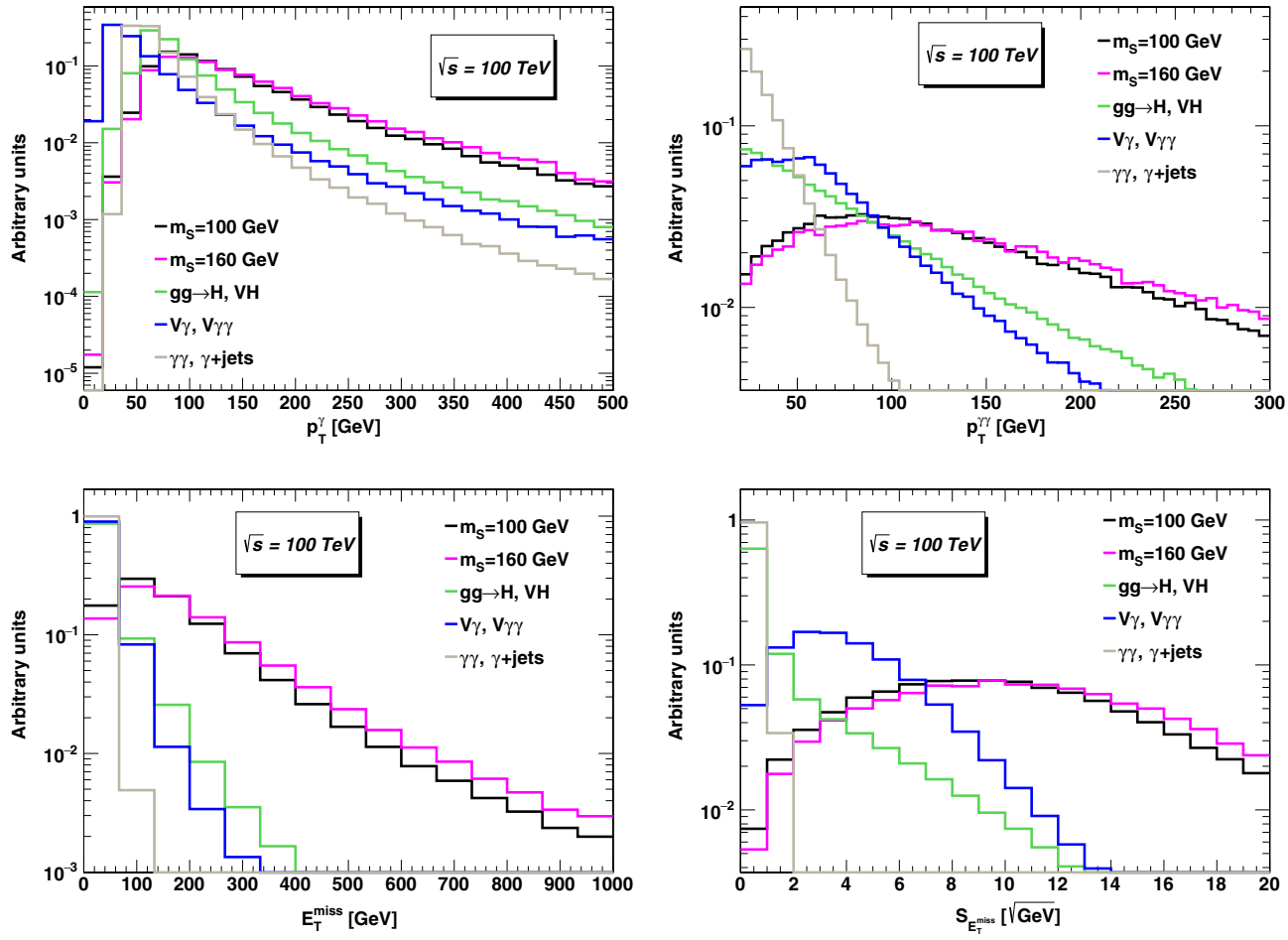

FIG. 10. Same as in Fig. 9 but for $\sqrt{s} = 100$ TeV.

$$S_{E_T^{\rm miss}} = \frac{E_T^{\rm miss}}{\sqrt{\sum_i E_T^i}}, \tag{22}$$

where i corresponds to all the objects (photons, jets, and leptons) used to construct the missing transverse energy. In addition, to improve the resolution of the $E_T^{\rm miss}$, tracks and clusters not associated with the diphoton primary vertex are not used to reconstruct $E_T^{\rm miss}$ [66]. The CMS Collaboration used variables that characterize the back-to-back event topology of the signal events [for instance, $|\Delta\Phi(E_T^{\rm miss}, \vec{p}_{\gamma\gamma})|$]. By requiring that such a quantity is larger than 2.1, only events where the reconstructed Higgs and missing transverse energy are back to back are selected. Therefore, the contribution from, e.g., $\gamma\gamma$ backgrounds is significantly reduced.

We compare the approaches used by ATLAS and CMS to reduce the contribution from $\gamma\gamma + \text{jets}$ backgrounds, on our benchmark points; we find that they produce results that agree with each other. We follow the ATLAS selection criteria throughout this study. We define two signal regions: the mono-Higgs signal region (denoted by the ATLAS signal region in this paper) and a tight signal region. The kinematical quantities and selection rules are displayed in Table V. In the two signal regions, we require that the invariant mass of the diphoton system falls inside the interval $[115, 135]$ GeV. Furthermore, we require that events contain no lepton (either electron or muon) with $p_T^\ell > 10$ GeV and $|\eta^\ell| < 2.5$.

At $\sqrt{s} = 14$ TeV, we can see from Table III that the signal-to-background ratio (S/B) can go from $\simeq 10^{-5}$ (after the first selection) to about $\simeq 1$ in the mono-Higgs signal region. In addition, the efficiency of the signal for $m_{H^0} = 100$ GeV is $A \times \epsilon \simeq 25\%$ in the ATLAS signal region. For the FCC-hh at 100 TeV, the signal-to-background ratio can go up to $\simeq 0.24$ in the tight signal region. If one requires, in addition to the tight selection rules, that $p_T^\gamma > 60$ GeV (for the leading photon) and $p_T^\gamma > 50$ GeV (for the subleading photon), the significance can increase to around $\simeq 20$ but the statistics goes down by about an order of magnitude.

V. RESULTS AND DISCUSSION

In Figs. 9 and 10, we display the normalized distributions of some key observables used in the

signal-to-background optimization. We can see that the p_T^γ of the leading photon is stronger for the signal than in the backgrounds, with a slightly high peak value for the signal case. The transverse momentum of the diphoton system (top right panel of Figs. 9 and 10) is a good discriminator. This can be understood as follows: The Higgs candidate (reconstructed from the two photons) is produced in association with heavy particles (resulting in a hard missing transverse energy spectrum), and therefore the corresponding recoil implies a harder p_T than in the backgrounds (especially SM Higgs backgrounds and $\gamma\gamma + \text{jets}$). The same observation applies to the E_T^{miss} (bottom left panel). The $S_{E_T^{\text{miss}}}$ shows a very important discriminatory power between the signal and the backgrounds. The condition used by the ATLAS Collaboration to define the mono-Higgs signal region ($S_{E_T^{\text{miss}}} > 7$) can be considered as an optimum. This is clear because requiring higher values for $S^{\text{min}}_{E_T^{\text{miss}}}$ will not only reduce the backgrounds but also diminish the signal. We report a difference between the results of our work and those in the ATLAS paper regarding the $S_{E_T^{\text{miss}}}$ and $p_T^{\gamma\gamma}$ variables; in the ATLAS paper, $\gamma\gamma$ and $\gamma + \text{jets}$ events can still have some contribution to these variables (in the hard region) due to the presence of pileup events (which are not taken into account in our analysis). However, the number of events is still not very important, e.g., about 10 events for $S_{E_T^{\text{miss}}} > 7$ at $\sqrt{s} = 13$ TeV and $\mathcal{L} = 36.5$ fb^{-1}. We can assign the differences in the modeling to an additional systematic uncertainty (see below).

To quantify the discovery potential of the signal, we estimate the significance defined by [134,135]

$$\mathcal{S} = \sqrt{2}\left[(s+b)\log\left(\frac{(s+b)(b+\delta_b^2)}{b^2+(s+b)\delta_b^2}\right) - \frac{b^2}{\delta_b^2}\log\left(1+\frac{\delta_b^2 s}{b(b+\delta_b^2)}\right)\right]^{1/2}, \tag{23}$$

where s and b refer to the number of signal and background events, respectively, and $\delta_b = xb$ is the uncertainty on the background events. Before discussing the results of our sensitivity projections, we comment on the possible sources of systematic uncertainties and their impact on the background contribution. First, there are uncertainties related to missing higher order corrections and PDF$+\alpha_s$. Uncertainties due to scale variations are usually determined by varying the renormalization and factorization by a factor of 2 in two directions, resulting in an envelope composed of nine possible variations (assuming no correlations with the PDF uncertainties). These uncertainties on the SM Higgs backgrounds are small due to the high precision calculations (2.5%–6% for $m_{\gamma\gamma}/\text{GeV} \in [110\!:\!160]$). Following the recommendation of the PDF4LHC working group [136], PDF $+ \alpha_s$ uncertainties can be estimated by combining both the variations of the same PDF set (used in the calculation of the cross section) with the variations due to alternative PDFs.[7] The size of the envelope spanned by all the variations defines the uncertainty due to PDF $+ \alpha_s$. In the signal region, such uncertainties are very small for SM Higgs backgrounds and can be of order 1.2%–2.5% [66]. An additional component of the theory uncertainty comes from the calculations of the $H \to \gamma\gamma$ branching ratio which is of order 1.73% [137]. The uncertainties on the nonresonant backgrounds can be larger than on the resonant backgrounds. In the analysis of [66], they were estimated directly from data and were of order 0.1%–9.8% in the $110 < m_{\gamma\gamma}/\text{GeV} < 160$ region. On the other hand, there are three major experimental uncertainties in the $\gamma\gamma + E_T^{\text{miss}}$ final state: luminosity, photon identification efficiency, and pileup reweighting. The total uncertainty on the background contribution including both resonant and nonresonant processes was estimated by the ATLAS Collaboration to be about 15%.[8] In this work, we compute the signal significance by taking into account the statistical uncertainty only or the statistical uncertainty in addition to a systematic uncertainty of order 5%, 10%, and 20%.

In Fig. 11, we plot the significance of the signal process at $\mathcal{L} = 3000$ fb^{-1} as a function of the dark Higgs mass m_{H^0} for both the HL-LHC and FCC-hh. We show the significance in the ATLAS mono-Higgs signal region (left panels) and in the signal region defined in our paper by the tight selection (right panels). We can see that masses up to 140 (160) GeV can be probed at the LHC (FCC-hh) if one assumes a total uncertainty of about 5%.

VI. CONCLUSIONS AND OUTLOOK

In this work, we carried out a complete study of the mono-Higgs signature in the scotogenic model in the limit of degenerate neutral scalars with a focus on the $\gamma\gamma$ final state at both the LHC-HL and FCC-hh. After revisiting the collider constraints from LEP and LHC run II, we have shown that a considerable region of the parameter space is still allowed, which is already excluded in general scenarios. Using the most significant benchmark points, we have shown that this model can be probed at the LHC-HL and the FCC-hh in the $H(\to\gamma\gamma) + E_T^{\text{miss}}$ channel with 3 ab^{-1} of integrated luminosity. The final state we considered has a small rate compared to the other production mechanisms of Majorana DM; however, due to the cleanliness of the $\gamma\gamma$

[7]According to the recommendations of PDF4LHC, the central PDF set is NNPDF30, while the two alternatives are CT10 and MMHT.

[8]The ATLAS Collaboration reported on the total error without specifying the contribution of systematic uncertainties. However, the CMS Collaboration [71] reported both the contribution of the statistical error which is the dominant one and the systematic error to the total uncertainty. In the signal region (defined as the high-p_T^{miss} in the CMS paper), the total systematic uncertainty is $\simeq$1.6%.

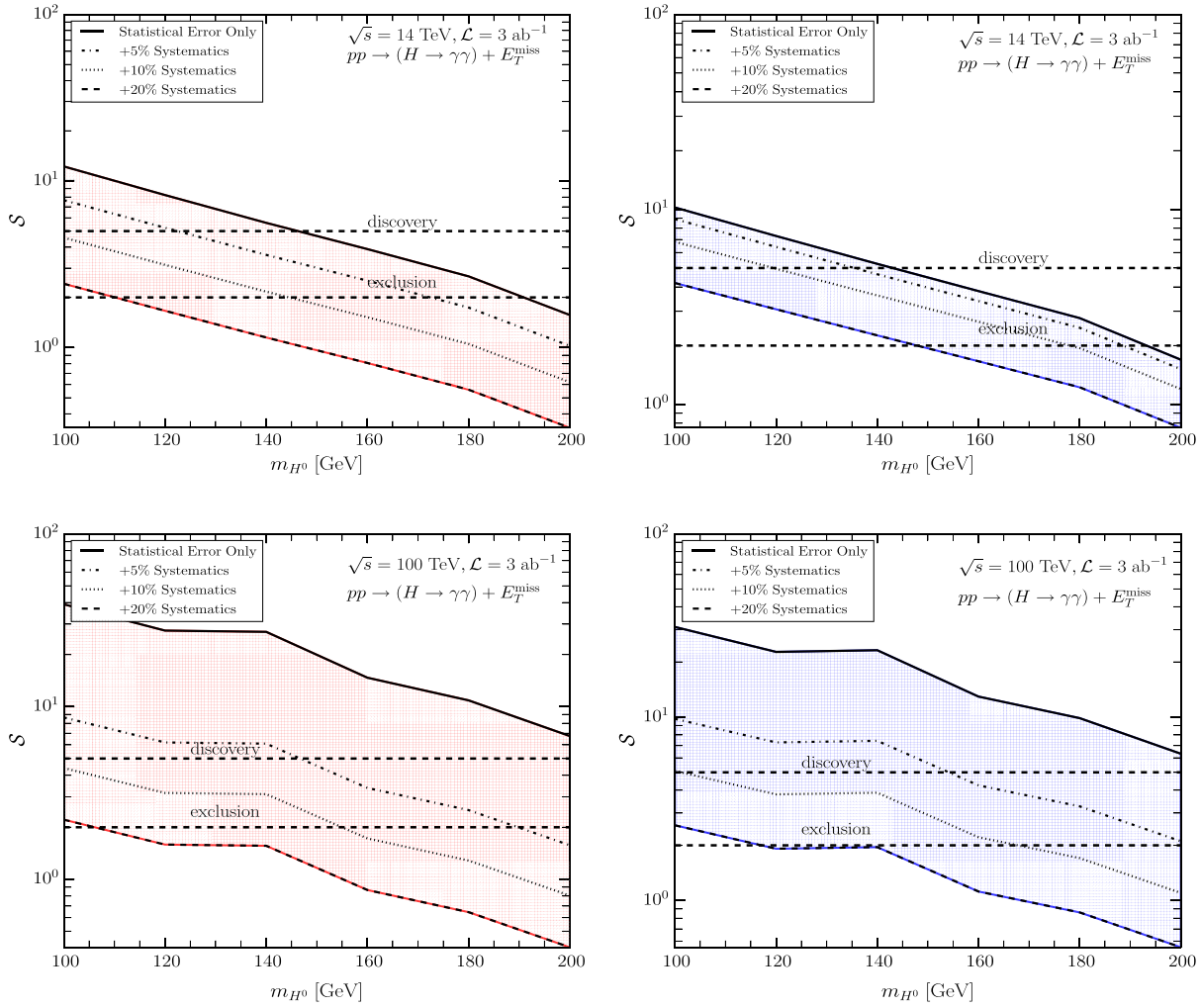

FIG. 11. Signal significance as a function of the dark Higgs mass m_{H^0} at $\int \mathrm{d}t\mathcal{L} = 3000$ fb^{-1} in the ATLAS mono-Higgs signal region (left panels) and after the tight selection (right panels) for the LHC at $\sqrt{s} = 14$ TeV (top panels) and for the FCC-hh at $\sqrt{s} = 100$ TeV (bottom panels). In all the panels, the solid line corresponds to the significance with the inclusion of the statistical uncertainty only, while dot-dashed, dotted, and dashed lines include a 5%, 10%, and 20% systematic uncertainty (summed in quadrature with the statistical error in the corresponding signal region).

decay channel and the high efficiency of photon identification at hadron colliders, we have shown that it can be used to probe our model. In summary, we have found that scalar masses up to 150 (160) GeV can be probed at the LHC (FCC-hh) assuming a 5% systematic uncertainty. We stress, however, that these results can be significantly improved by the use of multivariate techniques such as boosted decision tree or neural networks and by including other decay channels of the SM Higgs boson with larger branching fractions. We point out the importance of the mono-Higgs signature to probe the scalar coupling λ_L, which cannot be probed using, e.g., monojet searches of DM.

For the case of degenerate H^0/A^0 states, i.e., for $\lambda_5 \simeq 0$, and for $m_{H^\pm} = 95$ GeV, the dark scalars decay exclusively to a SM lepton (charged lepton or neutrino) and a Majorana fermion. Therefore, the mono-Higgs analysis itself is blind to the absolute values of the new Yukawa couplings as well as to the number of Majorana fermions with mass below the scalar dark Higgs ($m_{N_k} < m_{H^0}$). This conclusion can apply to all the production channels of dark scalars at hadron colliders. It is worth investigating the potential of other channels and observables to pin down such parameters. Below, we briefly discuss some methods to determine the new Yukawa couplings.

(i) *Higgs flavor violating decays*. The SM Higgs boson is expected to undergo lepton flavor violating decays in the scotogenic model. These decays are one-loop induced with the exchange of a charged scalar and Majorana fermions [Fig. 12(a)]. The ATLAS and the CMS collaborations have searched for these decays channels at $\sqrt{s} = 8 \oplus 13$ TeV (see, e.g., [138,139]).

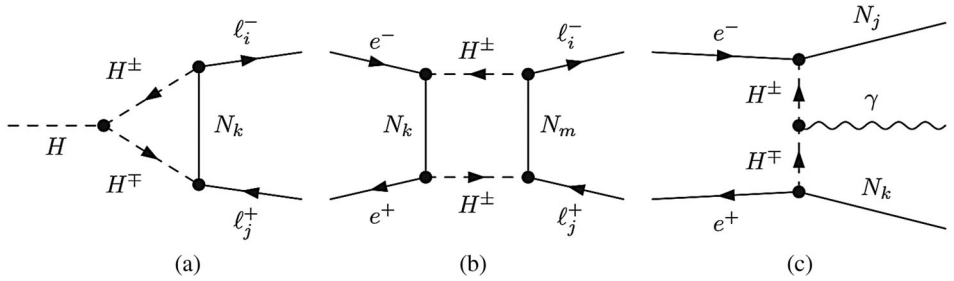

FIG. 12. Feynman diagrams of processes sensitive to the new Yukawa couplings. We show here the $H \to \ell_i \ell_j$, $i \neq j$ [diagram (a)], the one-loop induced $e^+e^- \to \ell_i^+ \ell_j^-$ [diagram (b)], and an example of direct production of Majorana fermions [diagram (c)].

The null results were used to put severe limits on the LFV Higgs decays, i.e., $\mathrm{BR}(H \to \mu\tau) < 0.25\%$ and $\mathrm{BR}(H \to e\tau) < 0.61\%$ [139]. Possibly observing one or more of these decay channels can be used to constrain one or several combinations of the new Yukawa coupling (these processes are also quadratically dependent on $g_{HH^\pm H^\pm} \propto \lambda_3$, which can still have large values).

(ii) *Precision measurement of lepton pair production at lepton colliders*. In the scotogenic model, a pair of charged leptons ($e^+e^- \to \ell_i^+ \ell_j^-$) can be produced with a decent rate at center-of-mass energies below or above the Z-boson pole [Fig. 12(b)]. Of these processes, the ones with $i \neq j$ are particularly interesting since they have almost zero cross section in the SM. Therefore, measurement of both inclusive and differential rates in $\ell_i^+ \ell_j^-$ can be used to extract several combinations of the new Yukawa couplings.

(iii) *Direct production at lepton colliders*. Inert scalars and Majorana fermions are the most sensitive channels of the new Yukawa couplings (they can also be used as model discriminators; see, e.g., [140]). Production of Majorana fermions (in association with photons, leptons, or Z bosons), either in the prompt mode or from the decay of dark scalars, is possible in the scotogenic model [in Fig. 12(c) we display an example of a Feynman diagram for $N_j N_k \gamma$ production].

ACKNOWLEDGMENTS

A. A. is supported by the Algerian Ministry of Higher Education and Scientific Research under the PRFU Project No. B00L02UN180120190003. A. J. would like to thank Robert V. Harlander for useful discussions, S. Banerjee for his help regarding the use of DELPHES, and F. Siegert for providing the correct setup of the calculation of the $\gamma +$ jets cross section in SHERPA. The work of A. A. was supported by the Moroccan Ministry of Higher Education and Scientific Research MESRSFC and CNRST: "Projet dans les domaines prioritaires de la recherche scientifique et du développement technologique": PPR/2015/6. The work of A. J. was supported in part by the Chinese Electron Positron Collider (CEPC) Theory Program and by the National Natural Science Foundation of China under Grants No. 11875189 and No. 11835005, and by the National Research Foundation of Korea, Grant No. NRF-2019R1A2C1009419. S. N. would like to acknowledge the support of the ICTP, where part of this work was done. The Feynman diagrams were drawn using JaxoDraw [141,142] and FeynArts [143].

APPENDIX: RECASTING OF LHC SEARCHES OF NEW PHYSICS AT $\sqrt{s} = 13$ TeV

In Sec. III, we studied the impact of the LHC searches of new physics beyond the SM on the parameter space of the scotogenic model with a Majorana dark matter. We discuss here the phenomenological setup of the event generation and a brief description of the analyses used in the reinterpretation effort. The analyses implemented in CheckMate are listed in Table I.

(i) atlas_conf_2016_050 [103]: The ATLAS Collaboration has searched for new phenomena in the final state consisting of $1\ell + (b)\mathrm{jets} + E_T^{\mathrm{miss}}$ at 13.3 fb^{-1} of luminosity. These searches focused on the supersymmetric partner of the top quark and also on DM production in association with a pair of top quarks. Upper bounds on the stop quark mass (for different assumptions regarding its decay branching ratios) were implemented. Furthermore, limits on DM simplified models were obtained and presented on a plane of the DM mass and pseudoscalar mediator mass for a coupling $g_{\mathrm{DM}} = 3.5$.

(ii) atlas_conf_2016_066 [104]: Using a data set corresponding to 13.3 fb^{-1} of luminosity, searches of new physics in the final state consisting of one photon, jets, and large E_T^{miss} is performed by the ATLAS Collaboration. These searches were used to probe supersymmetric models with gauge-mediated supersymmetry breaking, where neutralinos decay into a photon and a gravitino. Limits were put on the mass of a degenerate gluino state; i.e., $m_{\tilde{g}} > 1800$ GeV for a large range of neutralino (the next-to-lightest supersymmetric particle, NLSP, which is a mixture

of the Higgsino and the bino) masses and $m_{\tilde{g}} > 2000$ GeV for high neutralino mass.

(iii) atlas_conf_2016_076 [105]: A search of stop pair production and DM production in association with $t\bar{t}$ has been performed using 13.3 fb^{-1} of integrated luminosity. This search targeted final states composed of two charged leptons, jets, and large E_T^{miss}. From the nonobservation of a beyond-the-SM signal, 95% CL model-independent upper limits on the visible cross section were obtained (they vary between 0.38 fb and 1.18 fb depending on the analysis strategy).

(iv) atlas_conf_2017_060 [106]: Using a larger data set corresponding to 36.1 fb^{-1}, a search for new physics in the monojet final state ($1\,\text{jet} + E_T^{\text{miss}}$) is performed. Good agreement with the SM expectation was observed. As a consequence, exclusion limits on different models (with pair-produced weakly interacting DM candidates, large extra dimensions, and SUSY particles in several compressed scenarios) were obtained.

(v) atlas_1704_03848 [107]: A search for new physics in the monophoton final state ($1\gamma + E_T^{\text{miss}}$) with a data set corresponding to $\mathcal{L} = 36.1$ fb^{-1} was performed. Here, 95% CL limits were put on models with s-channel pseudoscalar mediators, effective field theory models, and on the production of a heavy Z' decaying into $Z(\to \nu\nu) + \gamma$.

(vi) atlas_1709_04183 [108]: A search for stop pair production was performed using the final state $0\ell + (n \geq 4)\text{jets} + E_T^{\text{miss}}$ at luminosity 36.1 fb^{-1}. The null searches were used to put exclusion limits on the top-squark and neutralino masses.

(vii) atlas_1712_02332 [108]: The final state consisting of (2–6) jets $+ E_T^{\text{miss}}$ at the luminosity 36.1 fb^{-1}, recorded by the ATLAS detector, was used to search for squarks and gluinos. Here, 95% CL lower limits on gluino masses ($m_{\tilde{g}} > 2.03$ TeV) and squark masses ($m_{\tilde{q}} > 1.55$ TeV) were implemented.

(viii) atlas_1712_08119 [110]: The final states with two low-momentum leptons and missing transverse momentum are used to search for electroweak production of SUSY particles in scenarios with compressed mass spectra at the luminosity 36.1 fb^{-1} recorded by ATLAS. Exclusion limits on SUSY particle masses are established.

(ix) atlas_1802_03158 [111]: Using 36.1 fb^{-1} of luminosity, photonic signatures (single photon and diphoton) in association with large E_T^{miss} are considered to look for SUSY particle production in generalized models of gauge-mediated supersymmetry breaking, using 36.1 fb^{-1} recorded by ATLAS. In these models, lower limits of 2.15 TeV, 1.82 TeV, and 1.06 GeV are set on the masses of gluinos, squarks, and a degenerate set of winos, respectively (for any value of the bino mass less than the mass of these produced states).

(x) cms_sus_16_025 [112]: The final state of two low-momentum opposite-sign leptons and missing transverse momentum in events recorded by CMS at luminosity 12.9 fb^{-1} of data collected at 13 TeV, to search for many new physics model candidates. The observed data yields are compatible with the SM predictions, and upper bounds of 175 GeV on charginos and the next-to-lightest neutralino are set, with a mass difference of 7.5 GeV with respect to the lightest neutralino.

(xi) cms_sus_16_039 [113]: Using the data recorded by CMS at 13 TeV and a luminosity 35.9 fb^{-1}, the final state of multileptons is considered to search for neutralinos and charginos that are weakly produced. In simplified SUSY models, these negative searches were interpreted as exclusions on the mass interval 180–1150 GeV.

(xii) cms_sus_16_048 [114]: Using the same CMS data set, the final state consisting of two low-momentum, oppositely charged leptons with missing transverse momentum is used to search for new physics. Negative search results implied exclusions on the winolike masses up to 230 GeV for a 20 GeV mass difference relative to the lightest neutralino, and the Higgsino-like masses are excluded up to 168 GeV for the same mass difference. In addition, the top squark masses up to 450 GeV are excluded for a mass difference of 40 GeV relative to the lightest neutralino.

Several processes in the scotogenic model are sensitive to these searches. These processes lead to different final states: $\ell^+\ell^- + E_T^{\text{miss}}$, $1\gamma + E_T^{\text{miss}}$, monojet, and $1\ell + \text{jets} + E_T^{\text{miss}}$ among others. First, charged Higgs boson pair production will lead to a final state composed primarily of two isolated charged leptons and a large E_T^{miss}. In some cases, where one charged lepton escapes the detection, this final state can be triggered as $1\ell + \text{jets} + E_T^{\text{miss}}$ where the jets are produced in initial-state radiation. For small mass splittings ($\Delta_{H^\pm} = m_{H^\pm} - m_{N_k}$), the missing transverse energy triggered by the Majorana fermion is even larger and thus gives high sensitivity. Production of a CP-odd (CP-even) dark scalar in association with a charged Higgs boson ($pp \to H^0 H^\pm$) leads exclusively to $1\ell + \text{jets} + E_T^{\text{miss}}$. We also considered the mono-V process with $V = W, Z$, which contributes to a final state composed of multijets ($n \geq 2$) and large transverse missing energy. On the other hand, monophoton and monojet processes are also possible in this model. For monojet production, we generated $S^0 S^0 + n$ jets ($S^0 = H^0, A^0$) using MadGraph5_aMC@NLO [127] with jet multiplicity up to three jets. We matched these inclusive samples using the MLM matching scheme [144]. PYTHIA 8.155 [145] was used for showering and hadronization. We have added by hand the PDG codes of

the three Majorana fermions (which should be considered as invisible particles) to the HCAL modules of the DELPHES card using the following commands:

```
add EnergyFraction 1000022 {0.0}
add EnergyFraction 1000023 {0.0}
add EnergyFraction 1000024 {0.0}
```

with the numbers inside the first brackets corresponding to the PDG codes of the Majorana fermions N_k.

[1] R. N. Mohapatra and G. Senjanovic, Neutrino Mass and Spontaneous Parity Violation, Phys. Rev. Lett. **44**, 912 (1980).

[2] J. Schechter and J. W. F. Valle, Neutrino masses in $SU(2) \times U(1)$ theories, Phys. Rev. D **22**, 2227 (1980).

[3] J. Schechter and J. W. F. Valle, Neutrino decay and spontaneous violation of lepton number, Phys. Rev. D **25**, 774 (1982).

[4] A. Zee, Charged scalar field and quantum number violations, Phys. Lett. **161B**, 141 (1985).

[5] E. Ma, Pathways to Naturally Small Neutrino Masses, Phys. Rev. Lett. **81**, 1171 (1998).

[6] A. Zee, Quantum numbers of Majorana neutrino masses, Nucl. Phys. **B264**, 99 (1986).

[7] K. S. Babu, Model of "calculable" Majorana neutrino masses, Phys. Lett. B **203**, 132 (1988).

[8] M. Aoki, S. Kanemura, T. Shindou, and K. Yagyu, An R-parity conserving radiative neutrino mass model without right-handed neutrinos, J. High Energy Phys. 07 (2010) 084; Erratum, J. High Energy Phys. 11 (2010) 49.

[9] G. Guo, X.-G. He, and G.-N. Li, Radiative two loop inverse seesaw and dark matter, J. High Energy Phys. 10 (2012) 044.

[10] Y. Kajiyama, H. Okada, and K. Yagyu, Two loop radiative seesaw model with inert triplet scalar field, Nucl. Phys. **B874**, 198 (2013).

[11] L. M. Krauss, S. Nasri, and M. Trodden, A model for neutrino masses and dark matter, Phys. Rev. D **67**, 085002 (2003).

[12] M. Aoki, S. Kanemura, and O. Seto, Neutrino Mass, Dark Matter and Baryon Asymmetry via TeV-Scale Physics without Fine-Tuning, Phys. Rev. Lett. **102**, 051805 (2009).

[13] M. Aoki, S. Kanemura, and O. Seto, A model of TeV scale physics for neutrino mass, dark matter and baryon asymmetry and its phenomenology, Phys. Rev. D **80**, 033007 (2009).

[14] M. Gustafsson, J. M. No, and M. A. Rivera, Predictive Model for Radiatively Induced Neutrino Masses and Mixings with Dark Matter, Phys. Rev. Lett. **110**, 211802 (2013); Erratum, Phys. Rev. Lett. **112**, 259902 (2014).

[15] A. Ahriche, C.-S. Chen, K. L. McDonald, and S. Nasri, Three-loop model of neutrino mass with dark matter, Phys. Rev. D **90**, 015024 (2014).

[16] A. Ahriche, K. L. McDonald, and S. Nasri, A model of radiative neutrino mass: With or without dark matter, J. High Energy Phys. 10 (2014) 167.

[17] H. Hatanaka, K. Nishiwaki, H. Okada, and Y. Orikasa, A three-loop neutrino model with global $U(1)$ symmetry, Nucl. Phys. **B894**, 268 (2015).

[18] K. Nishiwaki, H. Okada, and Y. Orikasa, Three loop neutrino model with isolated $k^{\pm\pm}$, Phys. Rev. D **92**, 093013 (2015).

[19] A. Ahriche, K. L. McDonald, S. Nasri, and T. Toma, A model of neutrino mass and dark matter with an accidental symmetry, Phys. Lett. B **746**, 430 (2015).

[20] A. Ahriche, K. L. McDonald, and S. Nasri, A radiative model for the weak scale and neutrino mass via dark matter, J. High Energy Phys. 02 (2016) 038.

[21] H. Okada and K. Yagyu, Three-loop neutrino mass model with doubly charged particles from isodoublets, Phys. Rev. D **93**, 013004 (2016).

[22] T. Nomura, H. Okada, and N. Okada, A colored KNT neutrino model, Phys. Lett. B **762**, 409 (2016).

[23] P.-H. Gu, High-scale leptogenesis with three-loop neutrino mass generation and dark matter, J. High Energy Phys. 04 (2017) 159.

[24] K. Cheung, T. Nomura, and H. Okada, Three-loop neutrino mass model with a colored triplet scalar, Phys. Rev. D **95**, 015026 (2017).

[25] K. Cheung, T. Nomura, and H. Okada, A three-loop neutrino model with leptoquark triplet scalars, Phys. Lett. B **768**, 359 (2017).

[26] B. Dutta, S. Ghosh, I. Gogoladze, and T. Li, Three-loop neutrino masses via new massive gauge bosons from E_6 GUT, Phys. Rev. D **98**, 055028 (2018).

[27] T. Nomura and H. Okada, Four-loop neutrino model inspired by diphoton excess at 750 GeV, Phys. Lett. B **755**, 306 (2016).

[28] N. G. Deshpande and E. Ma, Pattern of symmetry breaking with two Higgs doublets, Phys. Rev. D **18**, 2574 (1978).

[29] R. Barbieri, L. J. Hall, and V. S. Rychkov, Improved naturalness with a heavy Higgs: An alternative road to LHC physics, Phys. Rev. D **74**, 015007 (2006).

[30] E. Ma, Verifiable radiative seesaw mechanism of neutrino mass and dark matter, Phys. Rev. D **73**, 077301 (2006).

[31] M. Gustafsson, E. Lundstrom, L. Bergstrom, and J. Edsjo, Significant Gamma Lines from Inert Higgs Dark Matter, Phys. Rev. Lett. **99**, 041301 (2007).

[32] T. Hambye and M. H. G. Tytgat, Electroweak symmetry breaking induced by dark matter, Phys. Lett. B **659**, 651 (2008).

[33] P. Agrawal, E. M. Dolle, and C. A. Krenke, Signals of inert doublet dark matter in neutrino telescopes, Phys. Rev. D **79**, 015015 (2009).

[34] E. M. Dolle and S. Su, The inert dark matter, Phys. Rev. D **80**, 055012 (2009).

[35] S. Andreas, M. H. G. Tytgat, and Q. Swillens, Neutrinos from inert doublet dark matter, J. Cosmol. Astropart. Phys. 04 (2009) 004.

[36] E. Dolle, X. Miao, S. Su, and B. Thomas, Dilepton signals in the inert doublet model, Phys. Rev. D **81**, 035003 (2010).

[37] X. Miao, S. Su, and B. Thomas, Trilepton signals in the inert doublet model, Phys. Rev. D **82**, 035009 (2010).

[38] A. Arhrib, R. Benbrik, and N. Gaur, $H \to \gamma\gamma$ in inert Higgs doublet model, Phys. Rev. D **85**, 095021 (2012).

[39] A. Arhrib, Y.-L. S. Tsai, Q. Yuan, and T.-C. Yuan, An updated analysis of inert Higgs doublet model in light of the recent results from LUX, PLANCK, AMS-02 and LHC, J. Cosmol. Astropart. Phys. 06 (2014) 030.

[40] A. Goudelis, B. Herrmann, and O. Stål, Dark matter in the inert doublet model after the discovery of a Higgs-like boson at the LHC, J. High Energy Phys. 09 (2013) 106.

[41] A. Arhrib, R. Benbrik, and T.-C. Yuan, Associated production of Higgs at linear collider in the inert Higgs doublet model, Eur. Phys. J. C **74**, 2892 (2014).

[42] A. Arhrib, R. Benbrik, J. El Falaki, and A. Jueid, Radiative corrections to the triple Higgs coupling in the inert Higgs doublet model, J. High Energy Phys. 12 (2015) 007.

[43] H. Castilla-Valdez, A. Moyotl, M. A. Perez, and C. G. Honorato, Sensitivity of the decay $h \to ZZ^* \to Zl + l-$ to the Higgs self-coupling through radiative corrections, Phys. Rev. D **93**, 055001 (2016).

[44] S. Kanemura, M. Kikuchi, and K. Sakurai, Testing the dark matter scenario in the inert doublet model by future precision measurements of the Higgs boson couplings, Phys. Rev. D **94**, 115011 (2016).

[45] S. Banerjee and N. Chakrabarty, A revisit to scalar dark matter with radiative corrections, J. High Energy Phys. 05 (2019) 150.

[46] P. Poulose, S. Sahoo, and K. Sridhar, Exploring the inert doublet model through the dijet plus missing transverse energy channel at the LHC, Phys. Lett. B **765**, 300 (2017).

[47] F. P. Huang and J.-H. Yu, Exploring inert dark matter blind spots with gravitational wave signatures, Phys. Rev. D **98**, 095022 (2018).

[48] N. Wan, N. Li, B. Zhang, H. Yang, M.-F. Zhao, M. Song, G. Li, and J.-Y. Guo, Searches for dark matter via mono-W production in inert doublet model at the LHC, Commun. Theor. Phys. **69**, 617 (2018).

[49] A. Belyaev, T. R. F. P. Tomei, P. G. Mercadante, C. S. Moon, S. Moretti, S. F. Novaes, L. Panizzi, F. Rojas, and M. Thomas, Advancing LHC probes of dark matter from the inert 2-Higgs doublet model with the mono-jet signal, Phys. Rev. D **99**, 015011 (2019).

[50] A. Belyaev, G. Cacciapaglia, I. P. Ivanov, F. Rojas-Abatte, and M. Thomas, Anatomy of the inert two Higgs doublet model in the light of the LHC and non-LHC dark matter searches, Phys. Rev. D **97**, 035011 (2018).

[51] E. Lundstrom, M. Gustafsson, and J. Edsjo, The inert doublet model and LEP II limits, Phys. Rev. D **79**, 035013 (2009).

[52] G. Belanger, B. Dumont, A. Goudelis, B. Herrmann, S. Kraml, and D. Sengupta, Dilepton constraints in the inert doublet model from run 1 of the LHC, Phys. Rev. D **91**, 115011 (2015).

[53] N. Blinov, J. Kozaczuk, D. E. Morrissey, and A. de la Puente, Compressing the inert doublet model, Phys. Rev. D **93**, 035020 (2016).

[54] A. Ahriche, A. Jueid, and S. Nasri, Radiative neutrino mass and Majorana dark matter within an inert Higgs doublet model, Phys. Rev. D **97**, 095012 (2018).

[55] A. Merle and M. Platscher, Parity problem of the scotogenic neutrino model, Phys. Rev. D **92**, 095002 (2015).

[56] T. Kitabayashi, Scotogenic dark matter and single-zero textures of the neutrino mass matrix, Phys. Rev. D **98**, 083011 (2018).

[57] T. Hugle, M. Platscher, and K. Schmitz, Low-scale leptogenesis in the scotogenic neutrino mass model, Phys. Rev. D **98**, 023020 (2018).

[58] S. Baumholzer, V. Brdar, and P. Schwaller, The new νMSM ($\nu\nu$MSM): Radiative neutrino masses, keV-scale dark matter and viable leptogenesis with sub-tev new physics, J. High Energy Phys. 08 (2018) 067.

[59] D. Borah, P. S. B. Dev, and A. Kumar, TeV scale leptogenesis, inflaton dark matter and neutrino mass in a scotogenic model, Phys. Rev. D **99**, 055012 (2019).

[60] A. Vicente and C. E. Yaguna, Probing the scotogenic model with lepton flavor violating processes, J. High Energy Phys. 02 (2015) 144.

[61] L. Carpenter, A. DiFranzo, M. Mulhearn, C. Shimmin, S. Tulin, and D. Whiteson, Mono-Higgs-boson: A new collider probe of dark matter, Phys. Rev. D **89**, 075017 (2014).

[62] A. A. Petrov and W. Shepherd, Searching for dark matter at LHC with Mono-Higgs production, Phys. Lett. B **730**, 178 (2014).

[63] W. Abdallah, A. Hammad, S. Khalil, and S. Moretti, Search for mono-Higgs signals at the LHC in the B-L supersymmetric standard model, Phys. Rev. D **95**, 055019 (2017).

[64] K. Ghorbani and L. Khalkhali, Mono-Higgs signature in a fermionic dark matter model, J. Phys. G **44**, 105004 (2017).

[65] G. Aad *et al.* (ATLAS Collaboration), Search for Dark Matter in Events with Missing Transverse Momentum and a Higgs Boson Decaying to Two Photons in pp Collisions at $\sqrt{s} = 8$ TeV with the ATLAS Detector, Phys. Rev. Lett. **115**, 131801 (2015).

[66] M. Aaboud *et al.* (ATLAS Collaboration), Search for dark matter in association with a Higgs boson decaying to two photons at $\sqrt{s} = 13$ TeV with the ATLAS detector, Phys. Rev. D **96**, 112004 (2017).

[67] M. Aaboud *et al.* (ATLAS Collaboration), Search for dark matter in association with a Higgs boson decaying to b-quarks in pp collisions at $\sqrt{s} = 13$ TeV with the ATLAS detector, Phys. Lett. B **765**, 11 (2017).

[68] M. Aaboud *et al.* (ATLAS Collaboration), Search for Dark Matter Produced in Association with a Higgs Boson Decaying to $b\bar{b}$ using 36 fb^{-1} of pp collisions at $\sqrt{s} =$ 13 TeV with the ATLAS Detector, Phys. Rev. Lett. **119**, 181804 (2017).

[69] A. M. Sirunyan *et al.* (CMS Collaboration), Search for associated production of dark matter with a Higgs boson decaying to $b\bar{b}$ or $\gamma\gamma$ at $\sqrt{s} = 13$ TeV, J. High Energy Phys. 10 (2017) 180.

[70] A. M. Sirunyan *et al.* (CMS Collaboration), Search for dark matter produced in association with a Higgs boson decaying to a pair of bottom quarks in proton-proton collisions at $\sqrt{s} = 13$ TeV, Eur. Phys. J. C **79**, 280 (2019).

[71] A. M. Sirunyan *et al.* (CMS Collaboration), Search for dark matter produced in association with a Higgs boson decaying to $\gamma\gamma$ or $\tau^+\tau^-$ at $\sqrt{s} = 13$ TeV, J. High Energy Phys. 09 (2018) 046.

[72] S. P. Martin, Two loop effective potential for a general renormalizable theory and softly broken supersymmetry, Phys. Rev. D **65** (2002) 116003.

[73] Y. Cai, J. Herrero-García, M. A. Schmidt, A. Vicente, and R. R. Volkas, From the trees to the forest: A review of radiative neutrino mass models, Front. Phys. **5**, 63 (2017).

[74] J. A. Casas and A. Ibarra, Oscillating neutrinos and $\mu \to e\gamma$, Nucl. Phys. **B618**, 171 (2001).

[75] B. Pontecorvo, Neutrino experiments and the problem of conservation of leptonic charge, Zh. Eksp. Teor. Fiz. **53**, 1717 (1967) [Sov. Phys. JETP **26**, 984 (1968)].

[76] D. V. Forero, M. Tortola, and J. W. F. Valle, Global status of neutrino oscillation parameters after neutrino-2012, Phys. Rev. D **86**, 073012 (2012).

[77] A. Gando *et al.* (KamLAND-Zen Collaboration), Limit on Neutrinoless $\beta\beta$ Decay of ^{136}Xe from the First Phase of KamLAND-Zen and Comparison with the Positive Claim in ^{76}Ge, Phys. Rev. Lett. **110**, 062502 (2013).

[78] M. J. Dolinski, A. W. P. Poon, and W. Rodejohann, https://doi.org/10.1146/annurev-nucl-101918-023407.

[79] G. C. Branco, P. M. Ferreira, L. Lavoura, M. N. Rebelo, M. Sher, and J. P. Silva, Theory and phenomenology of two-Higgs-doublet models, Phys. Rep. **516**, 1 (2012).

[80] I. F. Ginzburg, K. A. Kanishev, M. Krawczyk, and D. Sokolowska, Evolution of Universe to the present inert phase, Phys. Rev. D **82**, 123533 (2010).

[81] S. Kanemura, T. Kubota, and E. Takasugi, Lee-Quigg-Thacker bounds for Higgs boson masses in a two doublet model, Phys. Lett. B **313**, 155 (1993).

[82] A. G. Akeroyd, A. Arhrib, and E.-M. Naimi, Note on tree level unitarity in the general two Higgs doublet model, Phys. Lett. B **490**, 119 (2000).

[83] M. E. Peskin and T. Takeuchi, Estimation of oblique electroweak corrections, Phys. Rev. D **46**, 381 (1992).

[84] W. Grimus, L. Lavoura, O. M. Ogreid, and P. Osland, The oblique parameters in multi-Higgs-doublet models, Nucl. Phys. **B801**, 81 (2008).

[85] C. Patrignani *et al.* (Particle Data Group Collaboration), Review of particle physics, Chin. Phys. C **40**, 100001 (2016).

[86] T. Toma and A. Vicente, Lepton flavor violation in the scotogenic model, J. High Energy Phys. 01 (2014) 160.

[87] J. Bernon and B. Dumont, Lilith: A tool for constraining new physics from Higgs measurements, Eur. Phys. J. C **75**, 440 (2015).

[88] S. Kraml, T. Q. Loc, D. T. Nhung, and L. D. Ninh, Constraining new physics from Higgs measurements with Lilith: Update to LHC Run 2 results, SciPost Phys. **7**, 052 (2019).

[89] A. M. Sirunyan *et al.* (CMS Collaboration), Combined measurements of Higgs boson couplings in proton–proton collisions at $\sqrt{s} = 13$TeV, Eur. Phys. J. C **79**, 421 (2019).

[90] G. Hinshaw *et al.* (WMAP Collaboration), Nine-year Wilkinson Microwave Anisotropy Probe (WMAP) observations: Cosmological parameter results, Astrophys. J. Suppl. Ser. **208**, 19 (2013).

[91] P. A. R. Ade *et al.* (Planck Collaboration), Planck 2015 results. XIII. Cosmological parameters, Astron. Astrophys. **594**, A13 (2016).

[92] E. Aprile *et al.* (XENON Collaboration), First Dark Matter Search Results From the XENON1T Experiment, Phys. Rev. Lett. **119**, 181301 (2017).

[93] S. M. Espirito, K. Hultqvist, P. Johansson, and A. Lipniacka, Search for neutralino pair production at $s**(1/2)$ from 192 to 208 GeV, DELPHI-002 PHYS 928, 2003.

[94] G. Abbiendi *et al.* (OPAL Collaboration), Search for anomalous production of dilepton events with missing transverse momentum in e^+e^- collisions at $\sqrt{s}$=183–209GeV, Eur. Phys. J. C **32**, 453 (2004).

[95] G. Abbiendi *et al.* (OPAL Collaboration), Search for chargino and neutralino production at $\sqrt{s} = 192$–209 GeV at LEP, Eur. Phys. J. C **35**, 1 (2004).

[96] J. Abdallah *et al.* (DELPHI Collaboration), Searches for supersymmetric particles in e^+e^- collisions up to 208 GeV and interpretation of the results within the MSSM, Eur. Phys. J. C **31**, 421 (2003).

[97] A. Pierce and J. Thaler, Natural dark matter from an unnatural Higgs boson and new colored particles at the TeV scale, J. High Energy Phys. 08 (2007) 026.

[98] M. L. Graesser and J. Shelton, Hunting Mixed Top Squark Decays, Phys. Rev. Lett. **111**, 121802 (2013).

[99] M. Drees, H. Dreiner, D. Schmeier, J. Tattersall, and J. S. Kim, CheckMate: Confronting your favourite new physics model with LHC data, Comput. Phys. Commun. **187**, 227 (2015).

[100] M. R. Buckley, J. D. Lykken, C. Rogan, and M. Spiropulu, Super-razor and searches for sleptons and charginos at the LHC, Phys. Rev. D **89**, 055020 (2014).

[101] D. Dercks, N. Desai, J. S. Kim, K. Rolbiecki, J. Tattersall, and T. Weber, CheckMate 2: From the model to the limit, Comput. Phys. Commun. **221**, 383 (2017).

[102] J. S. Kim, D. Schmeier, J. Tattersall, and K. Rolbiecki, A framework to create customised LHC analyses within CheckMate, Comput. Phys. Commun. **196**, 535 (2015).

[103] M. Aaboud *et al.* (ATLAS Collaboration), Search for top squarks in final states with one isolated lepton, jets, and missing transverse momentum in $\sqrt{s} = 13$ TeV pp collisions with the ATLAS detector, Phys. Rev. D **94**, 052009 (2016).

[104] ATLAS Collaboration, Search for supersymmetry in events with photons, jets and missing transverse energy with the ATLAS detector in 13 TeV pp collisions, CERN, Technical Report No. ATLAS-CONF-2016-066, 2016.

[105] ATLAS Collaboration, Search for direct top squark pair production and dark matter production in final states with two leptons in $\sqrt{s} = 13$ TeV pp collisions using 13.3 fb^{-1} of ATLAS data, CERN, Technical Report No. ATLAS-CONF-2016-076, 2016.

[106] M. Aaboud *et al.* (ATLAS Collaboration), Search for dark matter and other new phenomena in events with an

energetic jet and large missing transverse momentum using the ATLAS detector, J. High Energy Phys. 01 (2018) 126.
[107] M. Aaboud *et al.* (ATLAS Collaboration), Search for dark matter at $\sqrt{s} = 13$ TeV in final states containing an energetic photon and large missing transverse momentum with the ATLAS detector, Eur. Phys. J. C **77**, 393 (2017).
[108] M. Aaboud *et al.* (ATLAS Collaboration), Search for a scalar partner of the top quark in the jets plus missing transverse momentum final state at $\sqrt{s} = 13$ TeV with the ATLAS detector, J. High Energy Phys. 12 (2017) 085.
[109] M. Aaboud *et al.* (ATLAS Collaboration), Search for squarks and gluinos in final states with jets and missing transverse momentum using 36 fb^{-1} of $\sqrt{s} = 13$ TeV pp collision data with the ATLAS detector, Phys. Rev. D **97**, 112001 (2018).
[110] M. Aaboud *et al.* (ATLAS Collaboration), Search for electroweak production of supersymmetric states in scenarios with compressed mass spectra at $\sqrt{s} = 13$ TeV with the ATLAS detector, Phys. Rev. D **97**, 052010 (2018).
[111] M. Aaboud *et al.* (ATLAS Collaboration), Search for photonic signatures of gauge-mediated supersymmetry in 13 TeV pp collisions with the ATLAS detector, Phys. Rev. D **97**, 092006 (2018).
[112] CMS Collaboration, Search for new physics in the compressed mass spectra scenario using events with two soft opposite-sign leptons and missing momentum energy at 13 TeV, CERN, Technical Report No. CMS-PAS-SUS-16-025, 2016.
[113] A. M. Sirunyan *et al.* (CMS Collaboration), Search for electroweak production of charginos and neutralinos in multilepton final states in proton-proton collisions at $\sqrt{s} = 13$ TeV, J. High Energy Phys. 03 (2018) 166.
[114] A. M. Sirunyan *et al.* (CMS Collaboration), Search for new physics in events with two soft oppositely charged leptons and missing transverse momentum in proton-proton collisions at $\sqrt{s} = 13$ TeV, Phys. Lett. B **782**, 440 (2018).
[115] R. V. Harlander, S. Liebler, and H. Mantler, SusHi: A program for the calculation of Higgs production in gluon fusion and bottom-quark annihilation in the Standard Model and the MSSM, Comput. Phys. Commun. **184**, 1605 (2013).
[116] R. V. Harlander, S. Liebler, and H. Mantler, SusHi Bento: Beyond NNLO and the heavy-top limit, Comput. Phys. Commun. **212**, 239 (2017).
[117] K. G. Chetyrkin, J. H. Kuhn, and M. Steinhauser, RunDec: A Mathematica package for running and decoupling of the strong coupling and quark masses, Comput. Phys. Commun. **133**, 43 (2000).
[118] R. V. Harlander and W. B. Kilgore, Next-to-Next-to-Leading Order Higgs Production at Hadron Colliders, Phys. Rev. Lett. **88**, 201801 (2002).
[119] C. Anastasiou, C. Duhr, F. Dulat, E. Furlan, T. Gehrmann, F. Herzog, and B. Mistlberger, Higgs boson gluon-fusion production beyond threshold in N^{3}LO QCD, J. High Energy Phys. 03 (2015) 091.
[120] C. Anastasiou, C. Duhr, F. Dulat, E. Furlan, F. Herzog, and B. Mistlberger, Soft expansion of double-real-virtual corrections to Higgs production at N^{3}LO, J. High Energy Phys. 08 (2015) 051.
[121] C. Anastasiou, C. Duhr, F. Dulat, E. Furlan, T. Gehrmann, F. Herzog, A. Lazopoulos, and B. Mistlberger, High precision determination of the gluon fusion Higgs boson cross-section at the LHC, J. High Energy Phys. 05 (2016) 058.
[122] O. Brein, A. Djouadi, and R. Harlander, NNLO QCD corrections to the Higgs-strahlung processes at hadron colliders, Phys. Lett. B **579**, 149 (2004).
[123] M. L. Ciccolini, S. Dittmaier, and M. Kramer, Electroweak radiative corrections to associated WH and ZH production at hadron colliders, Phys. Rev. D **68**, 073003 (2003).
[124] O. Brein, R. Harlander, M. Wiesemann, and T. Zirke, Top-quark mediated effects in hadronic Higgs-strahlung, Eur. Phys. J. C **72**, 1868 (2012).
[125] O. Brein, R. V. Harlander, and T. J. E. Zirke, vh@nnlo—Higgs Strahlung at hadron colliders, Comput. Phys. Commun. **184**, 998 (2013).
[126] J. Gao, M. Guzzi, J. Huston, H.-L. Lai, Z. Li, P. Nadolsky, J. Pumplin, D. Stump, and C. P. Yuan, CT10 next-to-next-to-leading order global analysis of QCD, Phys. Rev. D **89**, 033009 (2014).
[127] J. Alwall, R. Frederix, S. Frixione, V. Hirschi, F. Maltoni, O. Mattelaer, H. S. Shao, T. Stelzer, P. Torrielli, and M. Zaro, The automated computation of tree-level and next-to-leading order differential cross sections, and their matching to parton shower simulations, J. High Energy Phys. 07 (2014) 079.
[128] R. D. Ball *et al.* (NNPDF Collaboration), Parton distributions for the LHC Run II, J. High Energy Phys. 04 (2015) 040.
[129] T. Gleisberg, S. Höche, F. Krauss, M. Schönherr, S. Schumann, F. Siegert, and J. Winter, Event generation with SHERPA 1.1, J. High Energy Phys. 02 (2009) 007.
[130] S. Catani, F. Krauss, R. Kuhn, and B. R. Webber, QCD matrix elements+parton showers, J. High Energy Phys. 11 (2001) 063.
[131] T. Sjöstrand, S. Ask, J. R. Christiansen, R. Corke, N. Desai, P. Ilten, S. Mrenna, S. Prestel, C. O. Rasmussen, and P. Z. Skands, An introduction to PYTHIA 8.2, Comput. Phys. Commun. **191**, 159 (2015).
[132] J. de Favereau, C. Delaere, P. Demin, A. Giammanco, V. Lemaître, A. Mertens, and M. Selvaggi (DELPHES 3 Collaboration), DELPHES 3, A modular framework for fast simulation of a generic collider experiment, J. High Energy Phys. 02 (2014) 057.
[133] M. Mangano, Physics at the FCC-hh, a 100 TeV pp collider, CERN Yellow Rep. Monogr. **3** (2017).
[134] G. Cowan, K. Cranmer, E. Gross, and O. Vitells, Asymptotic formulae for likelihood-based tests of new physics, Eur. Phys. J. C **71**, 1554 (2011); Erratum, Eur. Phys. J. C **73**, 2501 (2013).
[135] B. Coleppa, B. Fuks, P. Poulose, and S. Sahoo, Seeking heavy Higgs bosons through cascade decays, Phys. Rev. D **97**, 075007 (2018).
[136] J. Butterworth *et al.*, PDF4LHC recommendations for LHC Run II, J. Phys. G **43**, 023001 (2016).
[137] D. de Florian *et al.* (LHC Higgs Cross Section Working Group), Handbook of LHC Higgs cross sections: 4. Deciphering the nature of the Higgs sector, arXiv:1610.07922.

[138] G. Aad *et al.* (ATLAS Collaboration), Search for lepton-flavour-violating decays of the Higgs and Z bosons with the ATLAS detector, Eur. Phys. J. C **77**, 70 (2017).

[139] A. M. Sirunyan *et al.* (CMS Collaboration), Search for lepton flavour violating decays of the Higgs boson to $\mu\tau$ and $e\tau$ in proton-proton collisions at $\sqrt{s} = 13$ TeV, J. High Energy Phys. 06 (2018) 001.

[140] I. Maturana-Ávila, M. A. Díaz, N. Rojas, and S. Urrutia-Quiroga, Towards a way to distinguish between IHDM and the scotogenic at CLIC, arXiv:1903.11181.

[141] D. Binosi and L. Theussl, JaxoDraw: A graphical user interface for drawing Feynman diagrams, Comput. Phys. Commun. **161**, 76 (2004).

[142] D. Binosi, J. Collins, C. Kaufhold, and L. Theussl, JaxoDraw: A graphical user interface for drawing Feynman diagrams. Version 2.0 release notes, Comput. Phys. Commun. **180**, 1709 (2009).

[143] T. Hahn, Generating Feynman diagrams and amplitudes with FeynArts 3, Comput. Phys. Commun. **140**, 418 (2001).

[144] M. L. Mangano, M. Moretti, F. Piccinini, and M. Treccani, Matching matrix elements and shower evolution for top-quark production in hadronic collisions, J. High Energy Phys. 01 (2007) 013.

[145] T. Sjostrand, S. Mrenna, and P. Z. Skands, A brief introduction to PYTHIA 8.1, Comput. Phys. Commun. **178**, 852 (2008).